Lithos 115 (2010) 205–222

Contents lists available at ScienceDirect

Lithos

journal homepage: www.elsevier.com/locate/lithos

In situ U–Pb age determination and Nd isotopic analysis of perovskites from kimberlites in southern Africa and Somerset Island, Canada

Fu-Yuan Wu [a,*], Yue-Heng Yang [a], Roger H. Mitchell [b], Qiu-Li Li [a], Jin-Hui Yang [a], Yan-Bin Zhang [a]

[a] State Key Laboratory of Lithospheric Evolution, Institute of Geology and Geophysics, Chinese Academy of Sciences, Beijing 100029, China
[b] Department of Geology, Lakehead University, Thunder Bay, Ontario, Canada P7B 5E1

ARTICLE INFO

Article history:
Received 20 May 2009
Accepted 19 December 2009
Available online 4 January 2010

Keywords:
Laser ablation
U–Pb ages
Nd isotopes
Perovskite
Kimberlite
Southern Africa
Canada

ABSTRACT

Determination of the emplacement ages and initial isotopic composition of kimberlite by conventional isotopic methods using bulk rock samples is unreliable as these rocks usually contain diverse clasts of crustal- and mantle-derived materials and can be subject to post-intrusion sub-aerial alteration. In this study, 8 samples from 5 kimberlites in southern Africa and twelve samples from 7 kimberlites from Somerset Island, Canada have been selected for in situ perovskite U–Pb isotopic age determination and Nd isotopic analysis by laser ablation using thin sections and mineral separates. These fresh perovskites occur as primary groundmass minerals with grain-sizes of 10–100 μm. They were formed during the early stage of magmatic crystallization, and record data for the least contaminated or contamination-free kimberlitic magma. U–Pb isotopic data indicate that the majority of the southern Africa kimberlites investigated were emplaced during the Cretaceous with ages of 88 ± 3 to 97 ± 6 Ma, although one sample yielded an Early Paleozoic age of 515 ± 6 Ma. Twelve samples from Somerset Island yielded ages ranging from 93 ± 4 Ma to 108 ± 5 Ma and are contemporaneous with other Cretaceous kimberlite magmatism in central Canada (103–94 Ma). Although whole-rock compositions of the kimberlites from southern Africa have a large range of $\varepsilon_{Nd}(t)$ values (−0.5 to +5.1), the analysed perovskites show a more limited range of +1.2 to +3.1. Perovskites from Somerset Island have $\varepsilon_{Nd}(t)$ values of −0.2 to +1.4. These values are lower than that of depleted asthenospheric mantle, suggesting that kimberlites might be derived from the lower mantle. This study shows that in situ U–Pb and Nd isotopic analysis of perovskite by laser ablation is both rapid and economic, and serves as a powerful tool for the determination of the emplacement age and potential source of kimberlite magmas.

1. Introduction

Kimberlite is a unique ultrabasic rock derived from deep mantle, and is the major source of diamonds (Mitchell, 1986, 1995). The emplacement age and isotopic composition, combined with that of the entrained crustal and mantle xenoliths, is important for deciphering the composition and structure of the lithosphere at the time of eruption (Mitchell, 1986; Carlson et al., 2000). Precise determination of the emplacement age and isotopic composition is not simple, as kimberlites contain abundant crustal- and mantle-derived xenoliths and can undergo extensive alteration during sub-aerial weathering (Mitchell, 1986). Several isotopic methods have been used for kimberlite age determination (Allsopp et al., 1989). Although some reasonable data were obtained by Kramers and Smith (1983), whole-rock geochronology is now rarely used because of the presence of xenolithic material. The commonly used methods are mica (phlogopite) K–Ar, Ar–Ar and Rb–Sr age determinations (Smith et al., 1985). The common alteration, low closure temperature, and potential excess Ar render the K–Ar and Ar–Ar methods unreliable. With respect to the Rb–Sr isochron method, apart from the low closure temperature and effects of alteration, it is debatable whether or not all of the analysed phlogopites are cogenetic, as many crystals are undoubtedly xenocrysts. U–Pb and Th–Pb methods have been applied to zircon and baddeleyite (Davis et al., 1976). However, as shown by numerous studies (Kinny et al., 1989; Kinny and Meyer, 1994; Konzett et al., 1998; Belousova et al., 2001), zircons present in kimberlite are principally crustal- and/or mantle-derived xenocrysts. Both in situ and bulk analyses demonstrate that the U–Pb isotopic ages are typically older than the actual emplacement times of kimberlites (Kinny et al., 1989), suggesting that this method is not relevant to the determination of kimberlite emplacement ages (Allsopp et al., 1989).

On the basis of Sr–Nd isotopic data, trace and major element geochemistry, emplacement ages and mineral characteristics, kimberlites have been divided into Groups I (low initial Sr and high initial Nd isotope ratios) and II (high initial Sr and low initial Nd isotope ratios) (Smith, 1983), with an isotopically transitional type proposed by Nowell et al. (2004) and Becker et al. (2007). These groups were defined using data obtained by whole-rock analysis. However, as noted above, the combined effects of contamination and post-emplacement alteration implies that whole-rock analyses are not

* Corresponding author. Tel.: +86 10 82998217; fax: +86 10 62010846.
E-mail address: wufuyuan@mail.igcas.ac.cn (F.-Y. Wu).

0024-4937/$ – see front matter © 2009 Elsevier B.V. All rights reserved.
doi:10.1016/j.lithos.2009.12.010

representative of the isotopic composition of primary kimberlitic magma (Mitchell, 1986; Heaman, 1989).

Perovskite ($CaTiO_3$) is a common primary magmatic mineral in kimberlite, and has attracted much attention with regard to age and initial isotopic composition determination. Perovskite occurs in the groundmass of kimberlite and crystallizes at an early stage, together with magnesian chromite, and prior to the crystallization of monticellite, phlogopite, serpentine and calcite (Mitchell, 1972, 1986). It should therefore record the primary geochemical and isotopic signature with respect to the timing of emplacement and origin of the kimberlitic magma, prior to any contamination and weathering. Importantly, perovskite has high concentrations of Sr, U, Th, Zr, Hf and LREE (Jones and Wyllie, 1984; Mitchell, 1986; Mitchell and Reed, 1988; Heaman, 1989; Chakhmouradian and Mitchell, 2001a,b), making it an important mineral for U–Pb geochronology and Sr, Nd and Hf isotopic studies (Kramers and Smith, 1983; Allsopp et al., 1989; Smith et al., 1994; Kinny et al., 1997; Heaman et al., 2003, 2004; Cox and Wilton, 2006; Batumike et al., 2008; Eccles et al., 2008; Zurevinski et al., 2008). In particular, the high Sr content, coupled with low Rb (<2 ppm), and hence extremely low $^{87}Rb/^{86}Sr$ ratios (generally less than 0.001), also make perovskite an excellent candidate for Sr isotopic composition determination by laser ablation analysis (Paton et al., 2007a, b; Yang et al., 2008). The $^{87}Sr/^{86}Sr$ ratio obtained by this method can be considered as the initial Sr isotopic composition of the magma from which the perovskite crystallized, as the correction for in situ Rb decay is negligible. Recently, Nd isotopic compositional measurements by laser ablation have been successfully applied to perovskites from the Mengyin kimberlites of China (Yang et al., 2009).

Thus, perovskite is an important mineral for determining the age of emplacement and isotopic composition of the sources of kimberlitic magma. Although perovskite has the potential to be widely used for these purposes, its typical small size, usually 15–30 μm, makes the separation of pure mineral concentrates difficult. Moreover, recent studies have indicated that some perovskites exhibit both compositional zoning and alteration (Chakhmouradian and Mitchell, 2001a; Yang et al., 2009), making bulk analyses of multiple grains of doubtful value. In this paper, we report in situ U–Pb and Nd isotopic analyses of perovskite, in both thin sections and mineral separates, for kimberlites from southern Africa and Somerset Island, Canada. These data are used to demonstrate that precise crystallization ages and initial Nd isotopic compositions can be obtained from perovskite and can be of use in constraining the isotopic character of the mantle source of kimberlite magmas.

2. Geological setting and sample description

2.1. Southern African kimberlites

In southern Africa (Fig. 1a), kimberlites are principally intruded into the Kaapvaal craton (referred to as on-craton kimberlite) with minor occurrences in the Namaqua–Natal mobile belt (referred to as off-craton kimberlite). Kimberlites in this region have been divided into Groups I and II on the basis of their different Sr–Nd isotopic compositions (Smith, 1983), and their mineralogical character (Skinner, 1989). Mitchell (1995) has emphasized that the isotopic, geochemical and mineralogical distinctions of the groups are so different that they must represent different magma types derived from different sources. Hence, "Group I kimberlites" are best referred to simply as "kimberlite", whereas "Group II kimberlites", which are in fact *not* kimberlites but the distinct expression of lithospheric potassic magmatism in the Kaapvaal craton, should be termed "orangeites" (Mitchell, 1995) or "Kaapvaal metasomatized lithospheric mantle-derived magmas" (Mitchell, 2006).

Geochronological investigation of southern African kimberlites has been extensive and applied using a variety of methods (Allsopp et al., 1989, and references therein). The available data indicate these kimberlites were emplaced in several stages: 1600 Ma (Kuruman); 1200 Ma (Premier); 500 Ma (Zimbabwean); and 100–54 Ma (South Africa) (Allsopp et al., 1989; Shee et al., 1989; Jelsma et al., 2004); with the youngest the dominant period of emplacement.

The eight fresh southern African samples investigated are from five intrusions, and are without visible crustal fragments. Samples from the Kimberley area include: Wesselton Mine root zone hypabyssal rocks from kimberlite phases W3 and W2 collected at the 680 m level of the mine (W3-680, W2-680a, W2-680b and W2-680c); and an opaque-oxide rich zone (BF-18B) in the Benfontein Sill. The Ondermatjie (OND1-1) sample is a perovskite-rich hypabyssal dike rock from the Pofadder-Rietfontein area of South Africa. Samples from Thaba Putsoa (TP7) and Kao (Kao-K1, phase K1 or Gritty kimberlite of Clement (1973)) are hypabyssal and globular segregationary hypabyssal transitional kimberlites, respectively, from Lesotho.

The perovskites in these samples are typically euhedral with grain-sizes of 20–60 μm although some larger grains of up to 100 μm in size can be recognized (Fig. 2a, b, c and d). Perovskites in the Benfontein sample are larger than those in the Wesselton rocks, and exhibit well-defined compositional zoning (Fig. 2e and f). This sample also contains abundant baddeleyite as either inclusions within perovskite or individual grains (Fig. 2f, g and h). The Ondermatjie kimberlite consists of microphenocrysts of forsteritic olivine set in a fine-grained groundmass principally composed of resorbed perovskite (Fig. 2i and j), subhedral qandilite ulvospinel-magnetite, serpophitic serpentine and calcite. Being free of contamination by crustal rocks, it has been regarded as the Fe-rich end member of the spectrum of compositions proposed for primitive kimberlite magmas (Mitchell, 2004). The Kao K1 and Thaba Putsoa kimberlites contain fewer perovskite grains than those from South Africa, although some large grains up to 100 μm in size are present (Fig. 2k and l).

2.2. Somerset Island kimberlites

Somerset Island is considered to be part of the Churchill structural province of the Laurentian Shield (Fig. 1b), and is one of the Cretaceous kimberlite fields of North America (Mitchell, 1975; Heaman et al., 2004). Exploration indicates that at least 36 kimberlites occur in this area (Fig. 1b). Previous petrological studies indicated that most of the Somerset Island kimberlites belong to hypabyssal root zones (Mitchell and Meyer, 1980). The kimberlites contain diverse country rock and mantle-derived xenoliths and xenocrysts (Mitchell, 1977; Schmidberger and Francis, 1999, 2001; Schmidberger et al., 2001, 2002, 2003; Irvine et al., 2003). Although it was noted that the kimberlites in the area were emplaced during the Cretaceous with ages of 103–94 Ma (Heaman et al., 2004), precise age data are lacking. Thus, only a phlogopite Rb–Sr isochron from the Tunraq kimberlite with an age of 100 Ma has been reported (Smith et al., 1988).

Twelve samples from Somerset Island were selected for in situ analyses. Samples BND2-2 and C8 were investigated using thin sections whereas others were analysed using separated mineral fractions. Samples JP1-102, 103 and 104 are from the Nikos kimberlite, which exhibits a microporphyritic texture with phenocrysts of olivine, phlogopite, and spinel set in a very fine-grained carbonate-rich matrix. Perovskites occur in the groundmass associated with calcite, serpentine, and apatite, and have grain-sizes of 40–70 μm. Some perovskite grains exhibit thin mantles of ilmenite. Samples C8, PC-3 and PC-4 are from the Peuyuk kimberlite; this differs from the other kimberlites in the area in containing abundant crustal fragments and amoeboid lapilli (Mitchell and Fritz, 1973). Recently, Peuyuk C has been interpreted to be a pyroclastic kimberlite (Mitchell et al., 2009). Perovskites from these samples are small (30–60 μm) although larger grains can be rarely found (C8, Fig. 2n). Replacement by rutile is also common (Fig. 2n).The Tunraq (BND2-2 and Tunraq) kimberlite (Mitchell, 1979) is a mica-rich hypabyssal rock containing macrocrysts and phenocrysts of olivine and phlogopite, set in a very fine-grained carbonate-rich matrix consisting of spinel, calcite, serpentine, perovskite, and apatite. Calcite occurs as aggregates of tabular euhedral crystals or as sub-parallel laths,

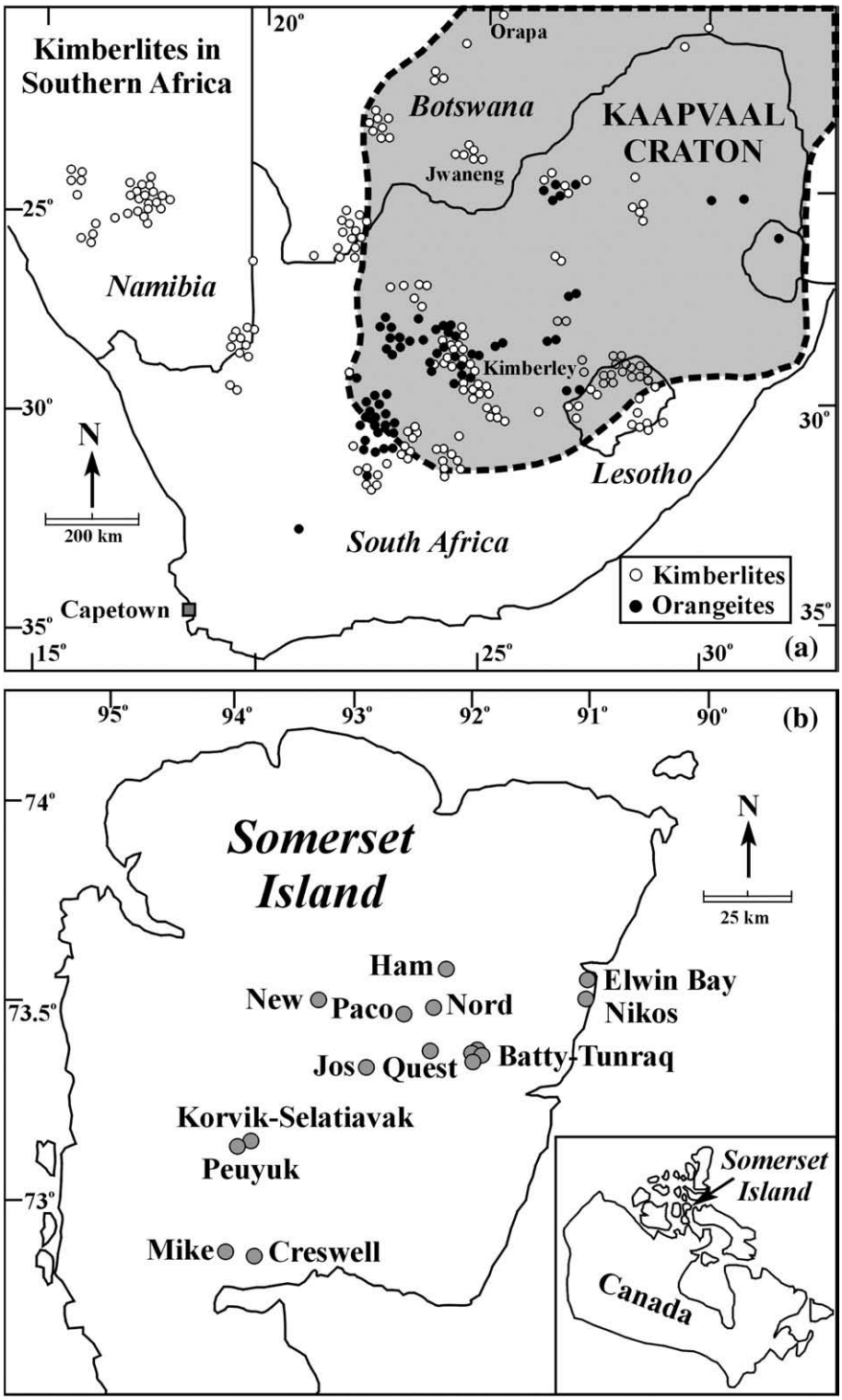

Fig. 1. Simplified distribution maps of kimberlites in southern Africa (a) (After Valley et al., 1998) and Somerset Island, Canada (b) (After Mitchell and Meyer, 1980; Schmidberger et al., 2001).

which are deflected around large olivine crystals, indicating their primary magmatic nature. Serpentine occurs as primary spherical microcrystalline segregations and as a retrograde alteration product of olivine. Perovskite occurs as discrete, zonation-free crystals or as grains mantled by Fe–Ti oxides with an average size of 10–50 μm (Fig. 2o). The other 4 samples (EL-6, Ham, Ama and BSD5-1) are from the Elwin, Ham, Amayersuk and Batty kimberlites, respectively. The perovskites in these samples are fresh and typically range in grain-size from 40–60 μm, although larger grains up to 100 μm in size are rarely found.

3. Analytical methods

Fresh kimberlite samples without visible crustal and mantle fragments were chosen for thin sections, and those containing large perovskite

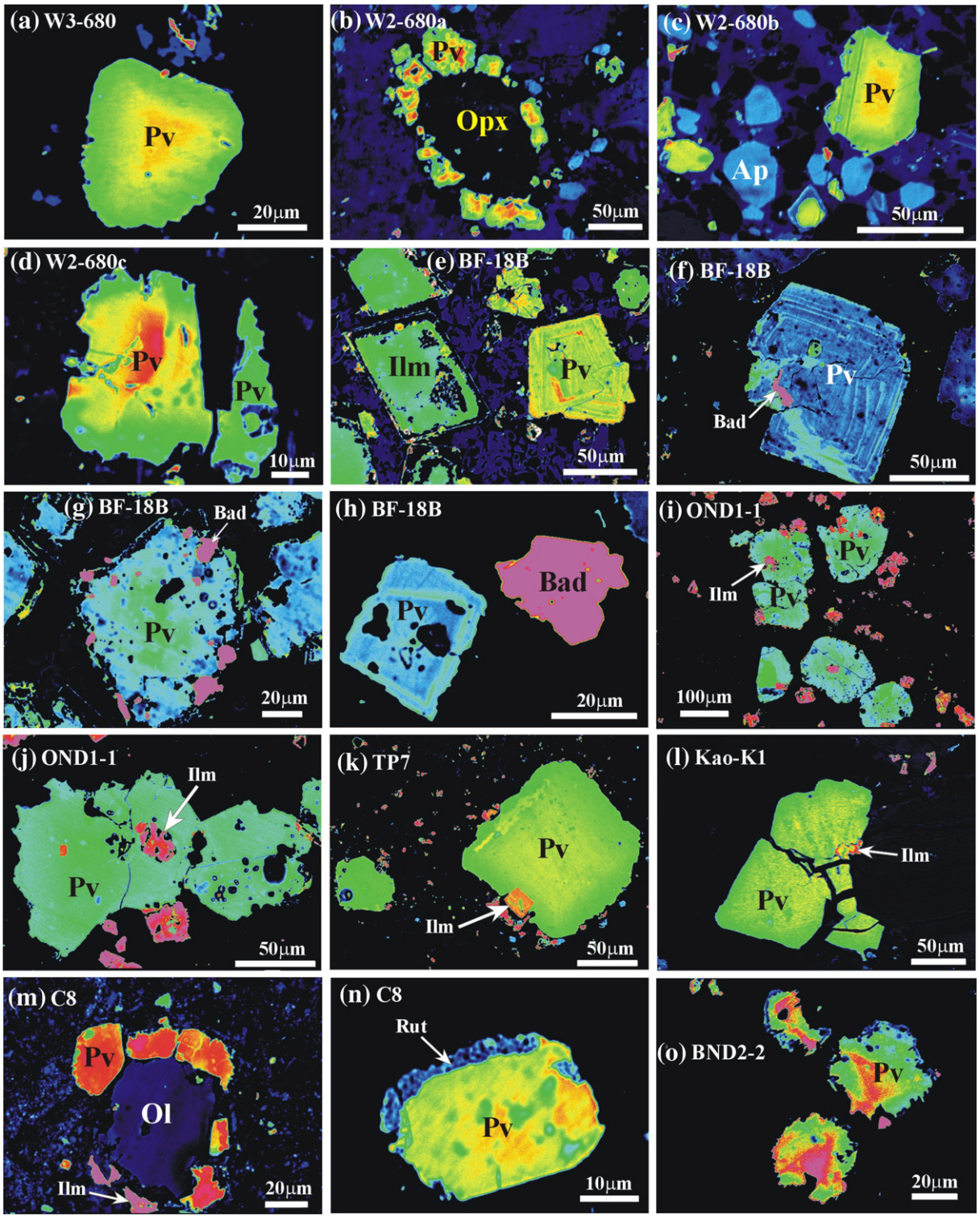

Fig. 2. False-color back-scattered electron (BSE) images of perovskites from southern African and Somerset Island kimberlites. (a) round perovskites (PV) with a grain-size of ~30 μm (Wesselton W3-680); (b) perovskite rim around orthopyroxene (Wesselton W2-680a); (c); irregular habit of perovskite (Wesselton W2-680b), with apatite; (d) anhedral perovskite (Wesselton W2-680c); (e) euhedral perovskite (Benfontein BF-18B); (f) euhedral and zoned perovskite and baddeleyite (Bad) inclusion (Benfontein BF-18B); (g) baddeleyite inclusions within the outer margin of perovskite (Benfontein BF-18B); (h) euhedral perovskite and baddeleyite; (i) euhedral perovskite with ilmenite inclusion (Ondermatje OND1-1); (j) ilmenite inclusions within perovskite (Ondermatje OND1-1); (k) euhedral perovskite (Thaba Putsoa TP7); (l) perovskite and ilmenite inclusion (Kao-K1); (m) perovskite rim around olivine (Ol); (n) rutile (Rut) rim around perovskite (Peuyuk C8) and (o) anhedral perovskite (Tunraq; BND2-2).

crystals were selected for in situ laser ablation. All analyses were undertaken at the Institute of Geology and Geophysics, Chinese Academy of Sciences, Beijing.

False-color back-scattered electron (BSE) images of perovskites were obtained using a *JEOL-JAX8100* microprobe with 15 kV accelerating potential and 12 nA beam current. Major element compositions

were obtained using this same instrument with counting times of 20 s. Total iron contents are expressed as Fe_2O_3.

Perovskite U–Pb and trace element compositions (including REE) were obtained using laser ablation inductively-coupled plasma mass spectrometry (LA-ICP-MS); detailed analytical procedures are described in Xie et al. (2008), thus only an outline is given here.

An ArF excimer laser ablation system (Geolas PLUS) was used for laser ablation analysis. This laser ablation system includes: (a) Lamda Physik Excimer laser COMPex 102 operated at 193 nm with a pulse width of ca. 15 nano-second; (b) Digitally-based software package from Digilaz™; (c) A laser optical system with a laser beam homogenizing system. The laser homogenizer consists of two 13×13 lens arrays, which can drill a perfectly cylindrical and flat-bottomed pit on the surface of the sample. The laser spot size can be adjusted to within 4–160 μm. The laser repetition rate was operated at 2–10 Hz depending on the signal intensity with a power density of ~20 J/cm^2. The ablation depth is estimated to be ~30–40 μm. With a 40 μm spot size and 4 Hz repetition rate, the volume of ablated material is estimated to be ~200,000 μm^3. Helium gas was flushed into the sample cell to minimize aerosol deposition around the ablation pit and argon gas was then used to improve transport efficiency.

The U–Pb analyses were conducted using an Agilent 7500a ICP-MS. During laser ablation, the sensitivity of ^{238}U of NIST SRM 610 is 14,000 cps/ppm using a spot size of 40 μm with laser repetition of 10 Hz and laser energy density of 25 J/cm^2. The mass stability is better than 0.05 amu/24 h. Before routine analysis, the P/A factor of the detector of the ICP-MS is corrected. It is also necessary to optimize instrumental parameters using a tuning solution in order to make the production of oxide (CeO^+/Ce^+) and doubly charged (Ce^{++}/Ce^+) less than 0.5% and 3%, and sensitivity better than 20 Mcps/ppm for ^{89}Y. The background of ^{204}Pb and ^{202}Hg was less than 100 cps because of the high purity of the argon and helium that were used. ICP-MS measurements were carried out using time-resolved analysis and peak hopping at one point per mass. The dwell time for each isotope was set at 6 ms for Si, Ca, Ti, Rb, Sr, Ba, Nb, Ta, Zr, Hf and REE, 15 ms for ^{204}Pb, ^{206}Pb, ^{207}Pb and ^{208}Pb and 10 ms for ^{232}Th and ^{238}U. Every 5 sample analyses were followed by one standard zircon 91500 and one NIST SRM 610 measurement. Each spot analysis consisted approximately of 30 s background acquisition and 40 s sample data acquisition.

In our analyses, ^{207}Pb/^{206}Pb, ^{206}Pb/^{238}U, ^{207}U/^{235}U (^{235}U = ^{238}U/137.88) and ^{208}Pb/^{232}Th ratios were corrected by using zircon 91500 as external standard. The fractionation correction and results were calculated using GLITTER 4.0 (GEMOC, Macquarie University). All the measured isotope ratios of zircon 91500 during the process of sample analysis were regressed and corrected using reference values. The relative standard deviations of reference values for zircon 91500 were set at 2%. However, unlike other commonly ablated minerals, such as zircon, baddeleyite and monazite, perovskites typically contain very high common Pb contents, in many cases amounting to >80% of the total Pb. This results in compositions being offset from Concordia in the U–Pb diagram. For this reason, a correction for common Pb is necessary to obtain precise ages for perovskites. Generally, four correction methods (i.e., ^{204}Pb, ^{206}Pb, ^{207}Pb and ^{208}Pb) can be employed for perovskite U–Pb age determination (Williams, 1998). For relatively young minerals, the ages are usually calculated from the ^{206}Pb/^{238}U ratios, and hence, the ^{206}Pb correction method is less used for the Phanerozoic minerals. Typically, a ^{204}Pb correction is applied in U–Pb geochronology using TIMS and SIMS analytical techniques (Heaman et al., 2003, 2004). For ICP-MS analyses by laser ablation, the ^{204}Pb contents cannot be precisely determined due to interference from a ^{204}Hg contaminant in the carrier gases, with the exception of analyses conducted using magnetic-field ICP-MS (Frei et al., 2008). In addition, the high Th contents make a ^{208}Pb correction inappropriate for perovskites (see details in Williams, 1998). Therefore, the ^{207}Pb correction is the most widely used method for perovskite common Pb corrections (Cox and Wilton, 2006). The precision of the ages determined using the ^{207}Pb correction method are much better than lower intercept ages, thus providing more reliable data for the emplacement age of kimberlite (Cox and Wilton, 2006). For this reason, the ^{207}Pb correction method is used in this study.

Alternatively, it is possible to obtain reasonable ages from perovskite using the Tera-Wasserburg (or normal) U–Pb diagram (e.g., Smith et al., 1989, 1994; Cox and Wilton, 2006; Batumike et al., 2008), in which data are considered to lie on a discordia line with the lower and upper intercepts defining the radiogenic and common Pb compositions (Williams, 1998). Alternatively, an isochron age can be obtained from a Pb–Pb diagram (Heaman, 1989; Smith et al., 1989; Corfu and Dahlgren, 2008). It is obvious that the discordia plot or chord to concordia represents mixing of two end-members. However, if all the analysed mineral grains contain almost the same proportions of radiogenic and common Pb, the analyses cluster together, and hence either no intercept age will be obtained, or an age with large error will be calculated (Frei et al., 2008), unless a regression to the common Pb composition is applied.

Therefore, in this study, the Tera-Wasserburg diagram was applied, in which the upper intercept to Concordia gives the common Pb composition and the lower intercept gives the crystallization age of mineral. In addition the ^{207}Pb method was applied for common Pb corrections using the common Pb composition obtained from the Tera-Wasserburg plot with ^{206}Pb/^{238}U weighted ages subsequently calculated using ISOPLOT 3.0 (Ludwig, 2003). Errors on individual analyses are based on counting statistics and are at the 1σ level, although errors on pooled ages are quoted at the 2σ or 95% confidence level. Trace element concentrations were calculated using GLITTER 4.0 and calibrated using ^{40}Ca as an internal standard, with NIST610 serving as an external reference material.

During laser analysis, potential problems are related to matrix effects. Due to the lack of an internationally-recognized perovskite reference standard, most laboratories use zircon standards for the external corrections (Cox and Wilton, 2006; Batumike et al., 2008), although an in-house perovskite standard can also be utilized (Frei et al., 2008). Of importance is that experiments have demonstrated that perovskite has the same fractionation characteristics as that of zircon during laser ablation (Cox and Wilton, 2006; Batumike et al., 2008); a conclusion verified by laser analyses of other materials (Horn et al., 2000; Cox et al., 2003; Horstwood et al., 2003; Košler et al., 2005; Storey et al., 2006; Vry and Baker, 2006; Chipley et al., 2007; Gregory et al., 2007). Therefore, it is concluded that matrix effects are not important for laser analyses of perovskite, and in particular using a 193 nm laser, which should induce little elemental fractionation as suggested by Guillong et al. (2003). During our analyses, no obvious differences in U/Pb fractionation are observed between zircon and perovskite (Fig. 3). Therefore, our perovskites ages are considered to be accurate with respect to the ages of kimberlite emplacement.

The in situ Nd isotopic analyses were undertaken using a Neptune MC-ICP-MS. A detailed description of the instrument and laser ablation system is presented in Wu et al. (2006); hence only a brief outline is given here. The mass spectrometer is a double-focusing multi-collector ICP-MS and has the capability of high mass resolution measurements in multiple collector mode. The present instrument is equipped with eight motorized Faraday cups and one fixed central channel, where the ion beam can be switched between a Faraday detector and an SEM detector. The external precision of the measurements is further improved by using a rotating amplifier concept, in which all Faraday cups are sequentially connected to all amplifiers, canceling out any gain calibration errors.

Nd isotopic measurements by solution and laser ablation using our Neptune machine have been described by Yang et al. (2007) and Yang et al. (2008), respectively. Using the exponential law for mass bias correction and assuming ^{146}Nd/^{144}Nd = 0.7219, the average ^{143}Nd/^{144}Nd ratios of the La Jolla Nd standard solution analysed over two years is 0.511849 ± 0.000014 (2SD, n = 68), which is identical, within error, to the recommended values of 0.511856– 0.511858 by MC-ICP-MS (Vance and Thirlwall, 2002). Before laser analyses, the La Jolla Nd

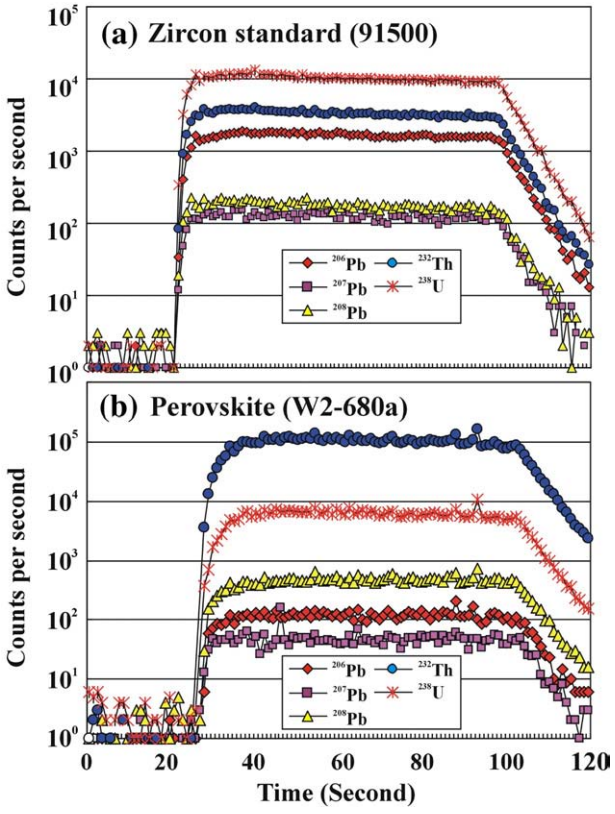

Fig. 3. Times vs count number of analysis of 91500 zircon (a) and perovskite W2-680a.

standard Nd solution was used to calibrate the machine and to evaluate the reproducibility and accuracy of the data.

Apart from the solution analyses, much attention was given to the potential isobaric interferences of ^{142}Ce on ^{142}Nd, ^{144}Sm on ^{144}Nd and ^{130}Ba^{16}O on ^{146}Nd. Our experiments and those of others show that the influence of ^{142}Ce on ^{142}Nd and ^{130}Ba^{16}O on ^{146}Nd are limited (Foster and Vance, 2006; Yang et al., 2007, 2008; McFarlane and McCulloch, 2007). In contrast, the isobaric interference of ^{144}Sm on ^{144}Nd cannot be neglected. In solution analyses, it is assumed that Sm has an identical mass bias to that of Nd, and thus the interference of ^{144}Sm on ^{144}Nd can be reasonably eliminated as only a small amount of Sm is present in the Nd fraction after chemical separation. However, it has been found that Sm and Nd have different and variable mass biases (β_{Sm} and β_{Nd}) (McFarlane and McCulloch, 2007; Yang et al., 2008), implying that the above-mentioned method is not feasible for laser ablation analysis. Therefore, the precise and accurate determination of the mass bias of Sm (β_{Sm}) is the key to obtaining reliable Nd isotopic data by laser analysis. Foster and Vance (2006) and Foster and Carter (2007) advocated an iterative approach for the Sm correction, in which the ^{146}Nd/^{144}Nd ratio is forced to converge to a stable value after several iterations for various Sm/Nd ratios prior to normalizing the ^{143}Nd/^{144}Nd ratio using the exponential law.

Recently, McFarlane and McCulloch (2007) proposed that the β_{Sm} value can be independently obtained from the measured versus true value of ^{147}Sm/^{149}Sm ratio. Then, the mass bias corrected ^{144}Sm/^{149}Sm ratio is used to correct the isobaric interference of ^{144}Sm on ^{144}Nd. Finally, mass bias corrections of interference-corrected ^{143}Nd/^{144}Nd and ^{145}Nd/^{144}Nd are independently applied using the canonical normalization of ^{146}Nd/^{144}Nd = 0.7219 (McFarlane and McCulloch, 2007).

In this study, the method of McFarlane and McCulloch (2007) is followed for our perovskite analyses. The recently revised ratios of ^{147}Sm/^{149}Sm (1.08680) and ^{144}Sm/^{149}Sm (0.22332) were applied to our data (Dubois et al., 1992; Isnard et al., 2005). After correction, the feasibility of our method was evaluated by comparing the ^{145}Nd/^{144}Nd ratio with the canonical value of 0.348415 as determined by TIMS (Wasserburg et al., 1981). During analyses, ^{147}Sm/^{144}Nd and ^{143}Nd/^{144}Nd ratios were calculated from the entire laser ablation process.

In order to evaluate measurements under different laser parameters, an apatite (1.5 cm × 1 cm × 0.5 cm) from Afghanistan was analysed with spot sizes of 60, 90 and 120 μm and repetition pulse rates of 6, 8 and 10 Hz. The data indicated that consistent Nd isotopic data can be obtained under various spot sizes and repetition pulses (Yang et al., 2008). The average ^{143}Nd/^{144}Nd ratio of the above 90 measurements was 0.511342 ± 31 (2SD), which agrees well with that of 0.511334 ± 10 (2SD, n = 8) obtained by purified solution MC-ICP-MS analyses. In addition, the average ^{145}Nd/^{144}Nd ratio of 90 measurements was 0.348424 ± 19 (2SD), identical to the recommended value.

As a further check for matrix effects, NIST 610 and perovskites from the Mengyin kimberlite of China were analysed. For the standard glass NIST 610, which has Sm and Nd concentrations of 441–460 and 429–442 ppm (Rocholl et al., 2000), with a Sm/Nd ratio of ~1.04 and ^{143}Nd/^{144}Nd ratios of 0.511908–0.511927 (Woodhead and Hergt, 2001; Foster and Vance, 2006), our fifteen analyses yielded an average ^{143}Nd/^{144}Nd ratio of 0.511910 ± 77 (2SD) or 0.511914 ± 18 (2σ) (Yang et al., 2008), identical to the values obtained by solution methods. For the Mengyin perovskites, the laser obtained average ^{143}Nd/^{144}Nd ratio from 15 analyses is 0.512229 ± 40 (2SD) or 0.512229 ± 11 (2σ), and thus similar to the ratio obtained by solution analyses (i.e. 0.512225–0.512235, Yang et al., 2008). These experiments indicate that matrix effects are negligible during laser Nd isotopic analyses. Moreover, the experiments suggested that reliable ^{143}Nd/^{144}Nd ratios can be obtained even for material in which the Sm/Nd is close to unity. In contrast, the Sm/Nd ratios of most natural geological materials are approximately 0.2–0.3. Although our experiments indicated that reliable Nd isotope data can be obtained using a spot size of 20 μm if the targeted mineral has Nd concentration of ~1000 ppm (Yang et al., 2008), a spot size of 40–60 μm with 4–10 Hz of pulse rate was used in this study.

4. Analytical results

4.1. Major and trace element composition of perovskite

The major and trace element data for the perovskites investigated are listed in Table 1 and rare earth element (REE) distribution patterns are shown in Fig. 4. These perovskites have similar compositions to those occurring in other kimberlites (Chakhmouradian and Mitchell, 2001a,b), in consisting mainly of TiO_2 (53.3–57.0 wt.%) and CaO (33.5–40.0 wt.%) with minor Fe_2O_3 (0.9–1.9 wt.%) and Na_2O (0.3–1.0 wt.%). With respect to trace elements, the perovskites are characterized by high concentrations of Sr (1097–2411 ppm), Nb (1837–8041 ppm), Ta (196–1186 ppm), Zr (476–3723 ppm), Hf (21–158 ppm), and minor Rb (0.5–52 ppm, typically <10 ppm). The REE distribution patterns show extreme light REE (LREE) enrichment with La abundances of about 10,000–25,000 times higher than those of chondrites and with $(La/Yb)_N$ ratios of 265–1131 (Fig. 4). The perovskites from southern Africa show larger REE variations ($(La)_N$ = 6361–26,236) than those from the Somerset Island ($(La)_N$ = 14,596–23,896) (Fig. 4).

4.2. Perovskite U–Pb isotopic ages

As shown by laser ICP-MS data (Table 1), perovskites have high U and Th contents that are favourable for U–Pb isotopic age determination. However, the high Pb contents require that a correction for common lead is necessary. For these perovskites, the ^{207}Pb correction method is applied, and the calculated ^{206}Pb/^{238}U weighted average age is provided (Table A1).

Table 1
Chemical compositions of the perovskites from S. Africa and Somerset Island.

	W3-680	W2-680a	W2-680b	NO#-WX	BF-18b	OND1-2	TP7	Kao-1b	JP1-102	JP1-103	JP1-104	C8	PC-03	PC-04	BND2-2	Tunraq	EL-6	Ham	Amayersuk	BSD5-1
Major elements (wt.%)																				
Number	11	5	6	9	9	5	8	10	13	12	10	6	11	9	5	11	7	9	11	11
SiO_2	0.04	0.04	0.03	0.08	0.03	0.03	0.00	0.01	0.08	0.05	0.07	0.06	0.05	0.07	0.03	0.05	0.03	0.11	0.01	0.03
TiO_2	54.91	53.67	53.91	54.93	53.26	56.34	57.00	56.83	55.34	55.59	54.33	53.30	54.23	54.48	54.78	55.49	54.09	54.25	53.86	54.48
Cr_2O_3	0.01	0.05	0.03	0.06	0.00	0.00	0.07	0.06	0.12	0.06	0.06	0.03	0.01	0.01	0.10	0.04	0.21	0.02	0.25	0.00
Al_2O_3	0.36	0.30	0.31	0.26	0.41	0.21	0.19	0.20	0.19	0.23	0.21	0.37	0.31	0.31	0.23	0.22	0.52	0.35	0.38	0.42
FeO	1.25	1.29	1.32	1.17	1.67	1.06	0.96	1.16	1.14	1.03	0.94	1.49	1.23	1.26	1.07	0.96	1.86	1.50	1.44	1.26
NiO	0.00	0.07	0.04	0.03	0.03	0.01	0.00	0.00	0.01	0.00	0.01	0.03	0.01	0.01	0.06	0.01	0.01	0.02	0.01	0.01
MnO	0.00	0.05	0.04	0.01	0.00	0.06	0.08	0.01	0.02	0.03	0.02	0.02	0.00	0.01	0.05	0.01	0.01	0.01	0.01	0.01
MgO	0.12	0.09	0.06	0.09	0.28	0.04	0.04	0.03	0.08	0.07	0.06	0.08	0.06	0.06	0.07	0.07	0.25	0.07	0.04	0.07
CaO	35.66	33.49	34.20	35.35	35.35	37.74	38.26	38.64	38.58	39.99	38.67	35.65	38.06	38.32	35.49	39.05	39.08	38.86	38.85	38.89
Na_2O	0.68	1.01	0.93	0.77	0.50	0.33	0.40	0.30	0.52	0.36	0.39	0.50	0.52	0.51	0.61	0.50	0.33	0.43	0.34	0.40
K_2O	0.04	0.06	0.05	0.02	0.02	0.04	0.01	0.00	0.02	0.01	0.02	0.04	0.01	0.02	0.04	0.02	0.02	0.02	0.01	0.01
Total	93.09	90.10	90.92	92.77	91.53	95.84	97.02	97.24	96.10	97.42	94.78	91.57	94.50	95.04	92.53	96.43	96.41	95.63	95.19	95.59
Trace elements (ppm)																				
Number	20	15	20	20	20	20	20	20	24	24	24	15	24	23	20	24	24	24	24	24
Rb	52.1	30.7	22.4	23.3	0.75	5.19	2.84	1.87	6.4	1.3	0.50	2.22	0.67	0.77	0.99	0.50	1.23	8.76	2.13	0.48
Sr	1837	1672	1548	1673	1692	1132	1097	1727	1663	1716	1635	1967	2232	2147	1787	1896	2156	2120	2411	2075
Ba	417	584	410	221	37.8	22.9	13.8	25.4	297	76	50	208	156	78.9	400	161	61.0	142	82.3	53
Nb	4843	5999	6019	4577	8041	1837	2565	2750	6828	5418	5036	5097	7223	6393	4467	5336	5876	7091	6958	6874
Ta	685	638	609	427	883	196	298	391	1186	793	711	685	1029	1133	417	688	847	881	968	938
Zr	1981	2775	3723	2528	2618	704	496	476	841	972	831	595	840	492	805	660	756	1155	980	1336
Hf	89.5	129.3	158	101	126	27.3	20.5	23.0	37	38	35.9	27.3	33.5	23.4	29.7	28.0	31.1	50.5	42.5	56.8
Pb	25.2	22.9	23.0	17.4	27.2	12.6	35.5	7.71	32	31	25.8	54.2	34.9	34.5	50.7	27.7	24.8	26.2	25.7	24.9
Th	3097	2672	2708	1345	2864	252	566	760	3670	2162	1958	3147	3812	4717	1418	2210	2391	2675	3056	3029
U	161	253	205	161	165	45.7	90.6	57.1	223	158	141	97.5	123	124	143	171	87.8	92.5	86.5	128
La	7150	7084	6754	5732	8264	2004	2619	3437	5170	4841	4591	6977	7042	6970	5209	5662	6138	6734	7527	7292
Ce	18,764	19,455	16,860	13,443	22,421	4583	5740	7997	13,242	11,548	10,909	15,610	16,083	16,754	11,191	12,499	14148	15,546	17,603	17,320
Pr	2227	2315	2002	1586	2721	548	652	983	1804	1565	1467	1683	2096	2184	1225	1645	1854	2005	2237	2189
Nd	8978	8979	8158	6472	10,869	2295	2613	3750	6639	5875	5454	6352	7574	7813	4636	5999	6682	7165	8050	8111
Sm	1179	1165	1067	884	1333	372	386	481	805	711	663	695	822	844	579	726	729	809	866	933
Eu	268	266	233	204	278	97.9	96.6	108	165	157	147	149	170	171	135	158	154	172	179	191
Gd	602	622	510	446	614	233	214	278	352	331	317	301	342	339	290	338	306	347	358	397
Tb	50.2	50.5	47.6	42.1	48.9	24.4	21.8	21.2	32	31	29.1	25.8	29.5	28.8	27.0	30.6	25.5	30.1	30.5	34.1
Dy	179	177	181	159	168	98.5	89.3	84.4	122	120	115	94.3	110	105	103	119	95	111	112	128
Ho	20.4	20.9	20.9	18.7	18.4	12.9	11.4	9.84	15	15	14.3	10.8	13.0	12.6	12.6	14.3	11.1	13.0	12.9	15.1
Er	30.3	30.7	33.5	29.8	27.1	21.2	19.7	16.2	23	24	22.4	17.5	20.4	19.4	20.5	23.1	17.5	19.7	20.1	23.7
Tm	2.34	2.46	2.66	2.29	2.00	1.77	1.67	1.29	1.96	2.11	1.94	1.38	1.64	1.56	1.71	1.94	1.37	1.68	1.57	1.91
Yb	9.73	10.4	11.3	10.1	8.24	7.57	7.60	5.53	8.18	8.57	8.50	6.17	6.72	6.68	7.75	7.81	5.61	6.66	6.45	7.98
Lu	0.75	0.82	0.94	0.82	0.66	0.64	0.67	0.47	0.76	0.81	0.78	0.52	0.60	0.60	0.70	0.79	0.51	0.56	0.58	0.77
Y	313	304	332	305	266	223	201	175	234	251	241	177	218	206	216	244	186	215	215	251
La/Yb	735	682	597	570	1003	265	345	622	632	565	540	1131	1048	1044	672	725	1094	1010	1168	914

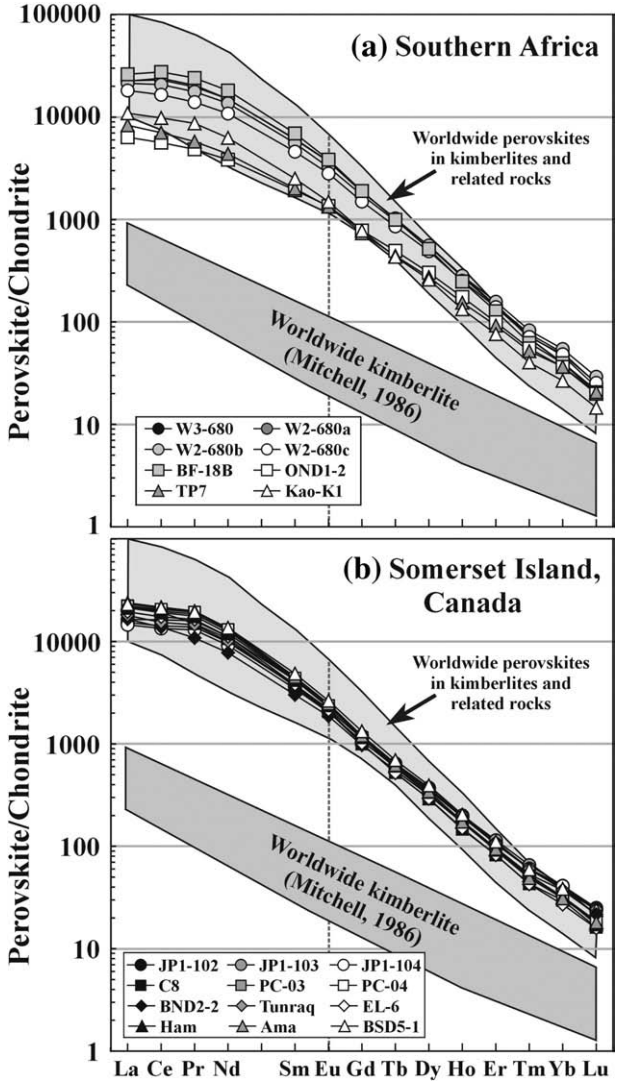

Fig. 4. Chondrite normalized REE distribution patterns of perovskites in kimberlites from southern Africa (a) and Somerset Island (b). The lower shaded area represents average compositions of kimberlites worldwide (Mitchell, 1986), and the upper one worldwide perovskites in kimberlites and related rocks (Mitchell and Reed, 1988; Melluso et al., 2008; Yang et al., 2009). The chondrite normalization values are 1.2 times less than those proposed by Masuda et al. (1973).

For the four kimberlite samples from Wesselton, the perovskites are mostly euhedral with grain-sizes ranging from 10 to 70 μm (Fig. 2a–d). Most of these perovskites have $^{207}Pb/^{206}Pb$ ratios of ~0.4 although some variations occur. The $^{206}Pb/^{238}U$ weighted average ages are 90 ± 2 Ma (W3-680, Fig. 5a), 89 ± 3 Ma (W2-680a, Fig. 5b), 90 ± 2 Ma (W2-680b, Fig. 5c) and 90 ± 3 Ma (W2-680c, Fig. 5d), i.e. they are identical within experimental errors. As expected perovskites from the Benfontein sill yielded a similar $^{206}Pb/^{238}U$ weighted average age of 88 ± 3 Ma (Fig. 5e). Ondermatjie perovskite, gives an age of 515 ± 6 Ma (Fig. 5f), identical to that of the Venetia kimberlite (519 ± 6 Ma; Phillips et al. (1999)). For kimberlites from Lesotho, perovskites from Thaba Putsoa and Kao-K1 yield $^{206}Pb/^{238}U$ weighted average ages of 89 ± 2 Ma (Fig. 5g) and 97 ± 6 Ma (Fig. 5h), respectively, identical to those from the Wesselton and Benfontein kimberlites.

With regard to kimberlites from Somerset Island, most perovskites have relatively higher $^{207}Pb/^{206}Pb$ ratios (0.4–0.7) than those from southern Africa (Fig. 6). Euhedral perovskites from three samples of the Nikos kimberlite give $^{206}Pb/^{238}U$ weighted average ages of 102 ± 3 (JP1-102, Fig. 6a), 102 ± 4 (JP1-103, Fig. 6b), and 100 ± 4 (JP1-104, Fig. 6c), respectively; identical within analytical error. Three samples from the Peuyuk kimberlite yielded $^{206}Pb/^{238}U$ ages of 108 ± 5 Ma (C-8, Fig. 6d), 97 ± 5 Ma (PC-3, Fig. 6e), and 107 ± 6 Ma (PC-4, Fig. 6f); i.e. consistent within error. Perovskites from the Tunraq kimberlite are euhedral with sizes ranging from 50 to 80 μm. Two samples from this kimberlite give $^{206}Pb/^{238}U$ weighted average ages of 93 ± 4 (BND2-2, Fig. 6g) and 100 ± 5 (Tunraq, Fig. 6h) and are thus identical within error. Samples from Elwin Bay, Ham, Amayersuk and Batty have $^{206}Pb/^{238}U$ weighted average ages of 103 ± 12 Ma (EL-6, Fig. 6i), 102 ± 13 Ma (Ham, Fig. 6j), 98 ± 8 Ma (Ama, Fig. 6k) and 98 ± 4 Ma (BSD5-1, Fig. 6l), respectively.

In order to check the veracity of our above laser ablation data, five perovskite samples from Somerset Island kimberlites were selected for SIMS analysis using a CAMECA 1280 installed at the Institute of Geology and Geophysics. Detailed descriptions of the instrument and analytical technique can be found in Li et al. (2009, 2010). Data for the analyzed perovskites are presented in Fig. 7 and Appendix Table A2. The calculated lower intercept ages are 110 ± 20 (JP1-102; laser age 102 ± 6), 85 ± 27 (PC-03; laser age 97 ± 10), 112 ± 16 (Tunraq; laser age 101 ± 9), 95 ± 22 (EL-6; laser age 98 ± 11), and 105 ± 18 (Ham; laser age 102 ± 20) Ma, respectively. If a ^{207}Pb correction is applied using the common Pb composition determined from the upper intercept, the $^{206}Pb/^{238}U$ weighted average ages are 110 ± 14 (JP1-102; laser age 102 ± 3), 85 ± 13 (PC-03; laser age 97 ± 5), 111 ± 10 (Tunraq; laser age 100 ± 5), 95 ± 11 (EL-6; laser age 98 ± 6), and 104 ± 10 (Ham; laser age 102 ± 13) Ma, respectively. It is noted that, for sample PC-3, the lower intercept and $^{206}Pb/^{238}U$ weighted ages are 104 ± 29 and 104 ± 18 Ma, respectively, if an outlier analysis is excluded (Fig. 7b). The ages obtained by SIMS analyses are identical to those by laser ablation technique within the analytical errors, although the former is evidently not as precise as the latter due to the fewer numbers of analyses.

4.3. Nd isotopic composition

The perovskites investigated have high REE concentrations with Sm and Nd ranging from 372 to 1333 and 2295 to 10,869 ppm, respectively (Table 1). Perovskites from Benfontein have the highest Sm and Nd contents (1333 and 10,869 ppm); whereas Ondermatjie perovskite has the lowest Sm and Nd contents (372 and 2295 ppm). Wesselton perovskites have Sm and Nd concentrations of 884–1179 and 6472–8979 ppm, respectively. Thaba Putsoa (TP7) and Kao (K1) perovskites have the lowest Sm and Nd concentrations, 386–481 and 2613–3750 ppm, respectively, of all the studied samples. In common with perovskite from Lesotho, the Somerset Island perovskites have low Sm and Nd concentrations of 579–933 and 4636–8111 ppm, respectively.

$^{147}Sm/^{144}Nd$ and $^{143}Nd/^{144}Nd$ ratios of perovskites are shown in Table A3 and Figs. 8 and 9, and summarized in Table 2. Overall, the perovskites from Somerset Island have slightly lower $^{147}Sm/^{144}Nd$ ratios (0.0692–0.0802) than those (0.0779–0.0912) from southern Africa (Table 2). The average $^{147}Sm/^{144}Nd$ ratios of the four samples from Wesselton are: 0.0854 (W3-680); 0.0831 (W2-680a); 0.0827 (W2-680b); and 0.0876 (W2-680c). Benfontein and Ondermatjie have the lowest and highest $^{147}Sm/^{144}Nd$ ratios of 0.0779 and 0.0993, respectively, of all samples from South Africa. The Thaba Putsoa and Kao perovskites have $^{147}Sm/^{144}Nd$ ratios of 0.0912 and 0.0834, respectively. Apart from Ondermatjie OND1-1, which is significantly older than others, the measured $^{143}Nd/^{144}Nd$ ratios range from 0.512552 to 0.512724. In terms of $\varepsilon_{Nd}(t)$ values (Table 2), six samples from South Africa show a narrow range of +1.2 to +2.3, whereas two samples from Lesotho give +2.2 (TP7) and +3.1 (Kao-1b). Relatively, the Somerset Island perovskites have slightly lower $\varepsilon_{Nd}(t)$ values of +1.0 to +1.4 with one exception of −0.2.

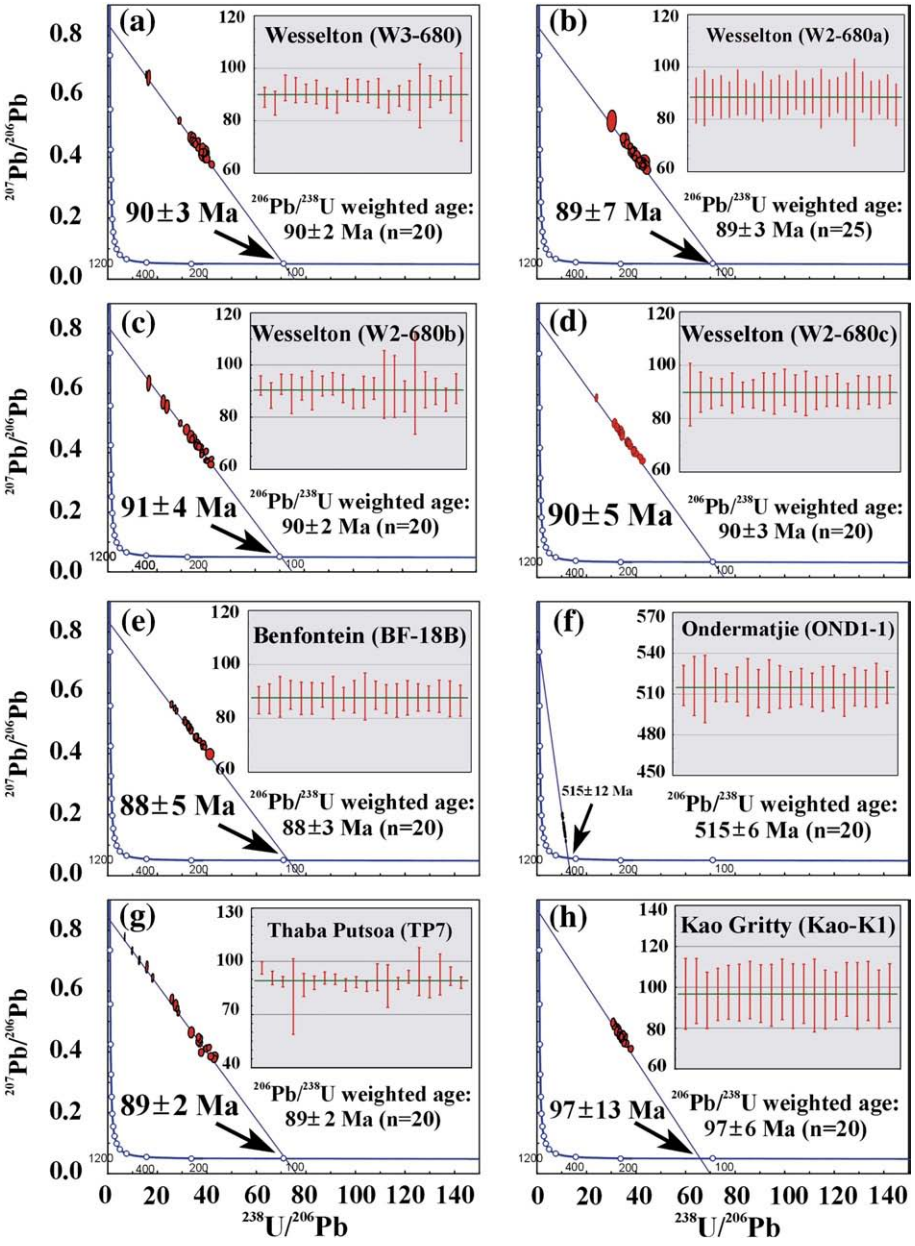

Fig. 5. U–Pb isotopic ages of perovskites obtained by laser ablation methods for kimberlites in southern Africa.

5. Discussion

5.1. Perovskite U–Pb age determination

As noted in the introduction and as shown in Fig. 10a, perovskites have high U concentrations (~30–300 ppm) compared to xenocrystal zircons in kimberlite (mostly <70 ppm), making this mineral an excellent candidate for U–Pb geochronology (Davis et al., 1976; Kramers and Smith, 1983; Smith et al., 1989, 1994; Kinny et al., 1997; Heaman et al., 2003, 2004; Cox and Wilton, 2006; Batumike et al., 2008; Zurevinski et al., 2008; Yang et al., 2009).

Following the methods of Dodson (1973) and Zhao and Zheng (2007), the calculated Pb closure temperatures of perovskite at different cooling rates are shown in Fig. 10b. Perovskite with a grain-size of 30–50 μm has a Pb closure temperatures of ~875–900 °C, i.e. ~100 °C lower than those of zircon of the same size. Kimberlites occur as small volume intrusions which crystallize rapidly and from the data given in Fig. 10b, we conclude the U–Pb age of perovskite can be used to constrain precisely the emplacement time of kimberlite.

However, perovskite differs significantly from other minerals used for U–Pb geochronology in its high common lead content which must be considered in the calculation of U–Pb ages. Regardless of which corrections are employed, it is necessary to know the composition of the common lead. Commonly, the two-stage growth curve model of Stacey and Kramers (1975) (simplified as SK model here) is applied (Kinny et al., 1997; Heaman et al., 2003, 2004; Zurevinski et al., 2008; Yang et al., 2009). Occasionally, common Pb compositions may not lie on the SK growth curve (Cox and Wilton, 2006), and in these cases, common lead composition must be determined from the upper intercept of the Tera-Wasserburg diagram. However, if all the analyses have little variation of Pb isotopic composition, and especially in the case of young perovskites which have not accumulated much radiogenic Pb, there are no means of determining the precise compositions of the common lead. In these cases, the SK model is the only method of determining the U–Pb age of perovskite although it can also be argued that kimberlitic magmas have different composition of common Pb to those predicted by the SK model.

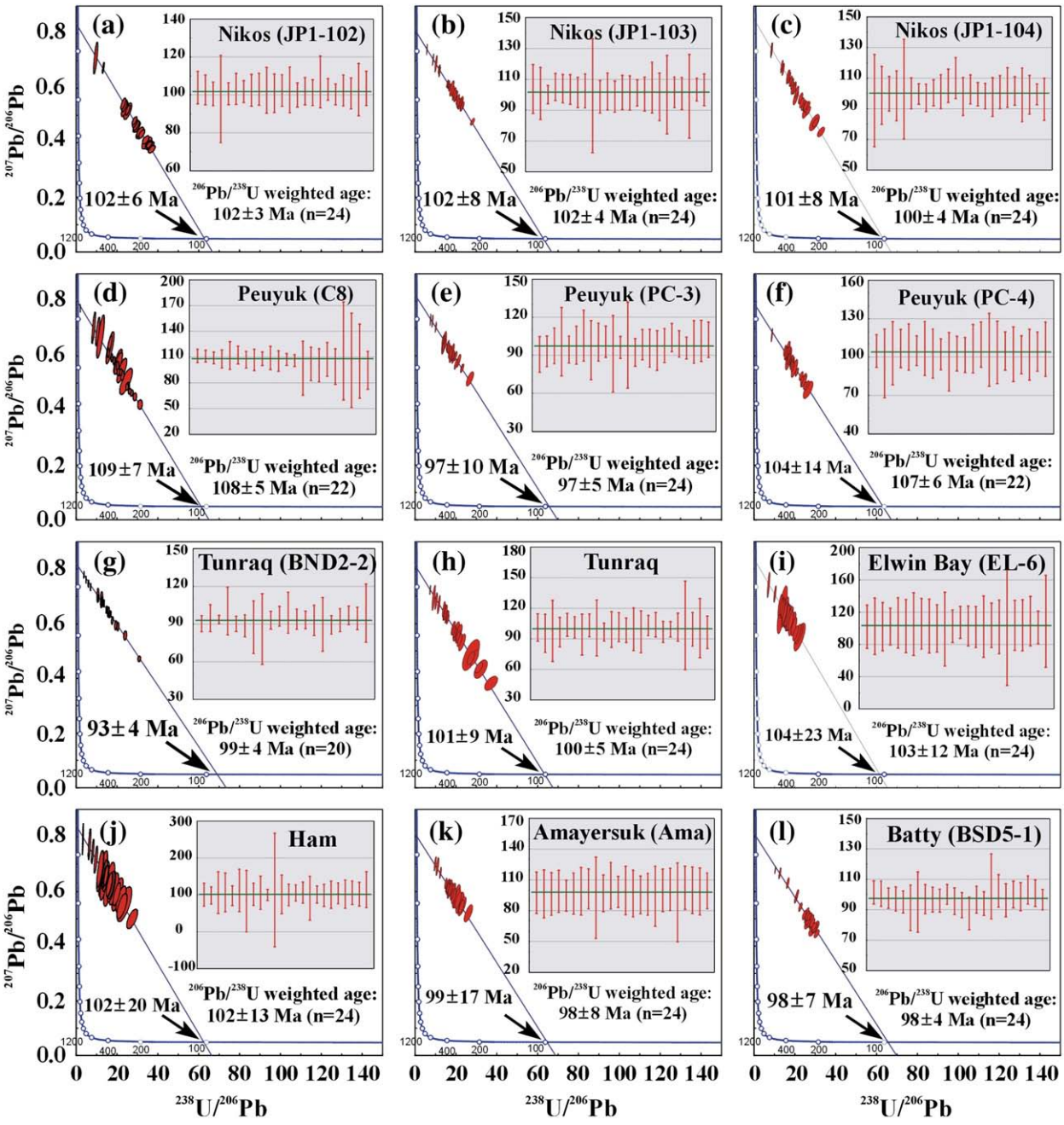

Fig. 6. U–Pb ages of perovskites obtained by laser ablation methods for kimberlites at Somerset Island, Canada.

We summarize all our ages calculated by different approaches and correction methods in Table 3. With respect to the ages calculated using ^{207}Pb corrections with common Pb compositions determined by the Tera-Wasserburg and SK model, respectively, the ages fall well within a ±10% uncertainty envelope, with the majority of the ages in agreement at the ±5% level (Fig. 11). The above observations suggest that the SK model can be reasonably used for perovskite U–Pb age calculation. This argument is also supported by consistency of ^{206}Pb/^{238}U and ^{208}Pb/^{232}Th ages when ^{204}Pb corrections were applied using the SK model. Therefore, we conclude there are no grounds for discarding the SK model for the perovskite U–Pb geochronology.

5.2. Emplacement ages of the studied kimberlites

For southern Africa, the ages of emplacement of most kimberlites have previously been obtained by phlogopite K (Ar)–Ar, Rb–Sr, and zircon U–Pb isotopic techniques (Allsopp et al., 1989; Zartman and Richardson, 2005), and also by perovskite U–Pb methods (Kramers and Smith, 1983; Smith et al., 1988, 1994; Batumike et al., 2008). Only the Cretaceous kimberlites are precisely dated by U–Pb isotopic analyses of perovskites. The 1600 Ma (Kuruman) and 1200 Ma (Premier) ages were determined by whole-rock Rb–Sr and Pb isotopic methods (Shee et al., 1989; Kramers and Smith, 1983), and the 100–54 Ma age of Jwaneng was obtained by phlogopite Rb–Sr and zircon U–Pb methods (Allsopp et al., 1989; Kinny et al., 1989). In the pioneer studies of perovskite age determination, Kramers and Smith (1983) and Smith et al. (1989) obtained numerous U–Pb ages for kimberlites in southern Africa.

Although the age precision of these previous estimates was not satisfactory, due to limited analytical fractions, the ages for kimberlites at Wesselton, Dutoitspan, Bultfontein, De Beers, Monastery and Goedgevonden are Cretaceous (60–117 Ma). Kimberlites from Beit

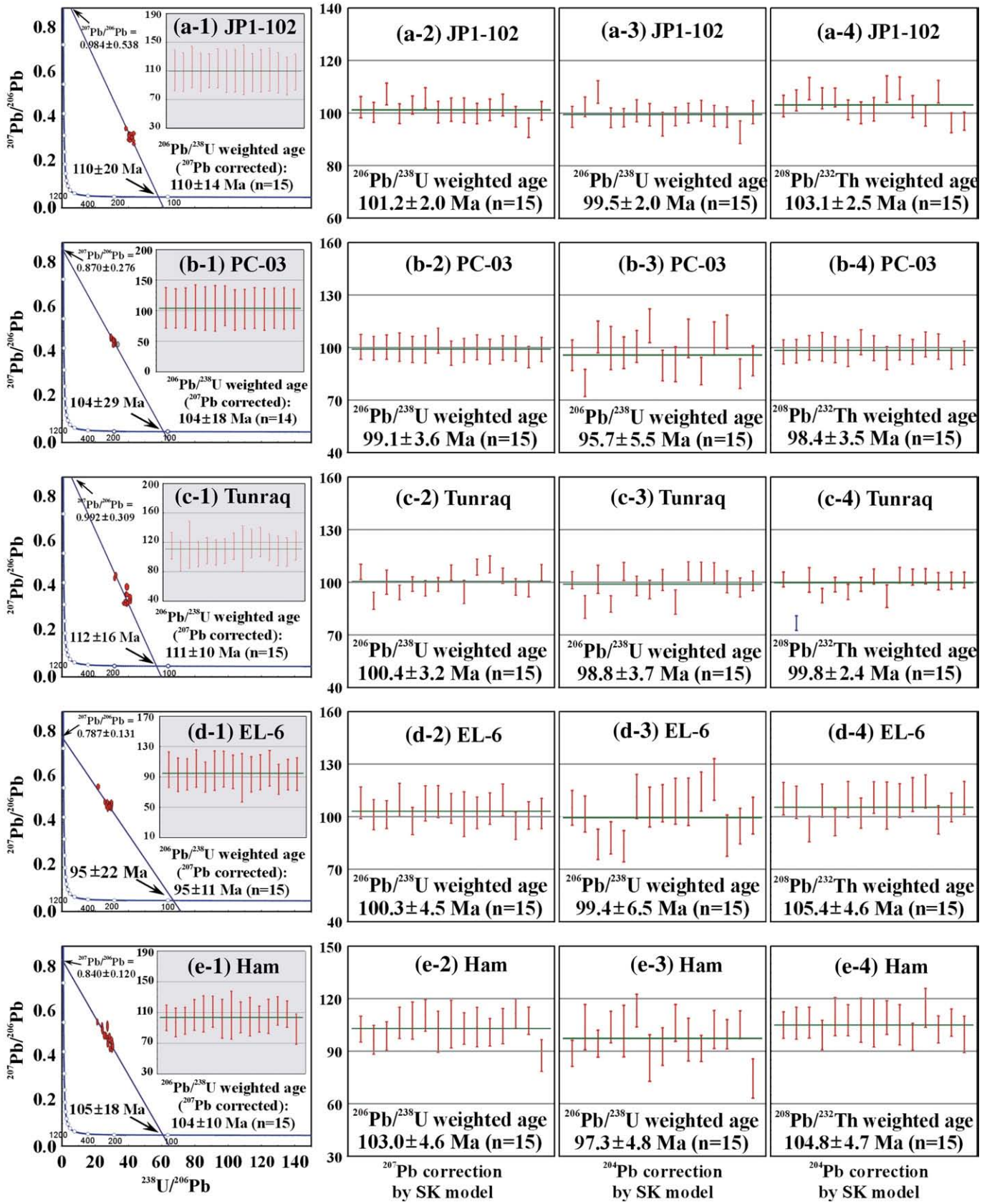

Fig. 7. U–Pb ages of perovskites obtained by CAMECA 1280 SIMS.

Bridge and Colossus in Zimbabwe yield a broad age variation from 310 to 740 Ma with large errors. Subsequently, Smith et al. (1994) provided four U–Pb isotopic ages from 100 to 140 Ma for perovskites from kimberlites in the Prieska region of South Africa. Recently, Batumike et al. (2008) investigated five kimberlites in South Africa, including Wesselton, Benfontein, DeBeers and Monastery, and

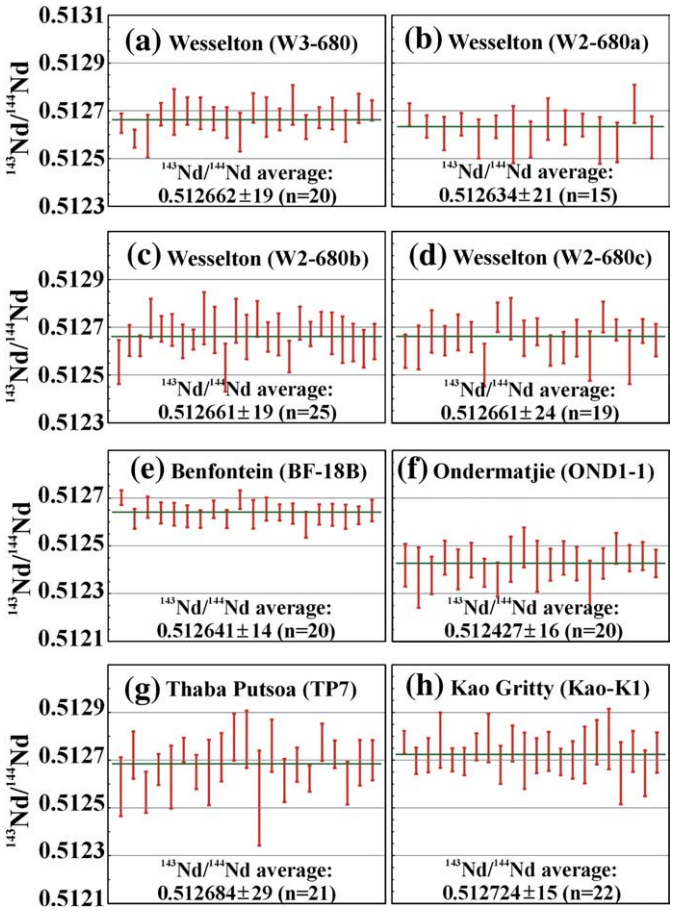

Fig. 8. Nd isotopic compositions of perovskites from kimberlites in southern Africa.

obtained ages from 86.0 ± 2.7 to 88.6 ± 5.9 Ma. In addition, Eocene and Quaternary ages were also found for kimberlites in Tanzania and the Democratic Republic of Congo (Batumike et al., 2008).

In this study, the age of 515 ± 6 Ma for the Ondermatje kimberlite confirms the existence of Pan-African kimberlitic emplacement, and is identical with that of the Venetia kimberlite (519 ± 6 Ma, Phillips et al. (1999)). The other southern African samples show a limited range of U–Pb ages (88 ± 3–97 ± 6 Ma), comparable to data obtained previously (Smith et al., 1989; Batumike et al., 2008). For the Wesselton kimberlites, four samples of perovskites in this study yield ages of 88.5 ± 3.0 to 90.4 ± 2.2 Ma, consistent with that reported by Batumike et al. (2008). For the Benfontein sill, our perovskite U–Pb age is 88 ± 3 Ma, identical to the age of 86.0 ± 2.7 Ma (if a ^{207}Pb correction is applied this age would be 90 ± 2 Ma) of Batumike et al. (2008). These consistencies also indicate that our methods are valid since the same correction methods are applied in both studies. In Lesotho, the kimberlites have not been extensively investigated and Kramers and Smith (1983) have reported a whole-rock Pb isotopic age of 89 ± 14 Ma for Kao pipe. Kimberlites investigated in this study give more precise age from 89 ± 2 to 97 ± 6 Ma.

The ages of kimberlites from Somerset Island, Canada, were not well constrained before this study. Kramers and Smith (1983) reported an age of 105–110 Ma for the Georgia melnoite, and a much younger age of ~40 Ma for the Elwin Bay kimberlite. The latter was considered to result from later Pb loss and/or U gain, and is clearly discrepant relative to our data. In our study, three samples from the Nikos kimberlites have ages of 100 ± 4 to 102 ± 4 Ma, and three samples from Peuyuk have ages of 97 ± 5 to 108 ± 5 Ma. Two samples from the Tunraq kimberlite give perovskite U–Pb ages of 93 ± 4 and 100 ± 10 Ma. These ages are identical to the Rb–Sr phlogopite age of 100 Ma obtained by Smith et al. (1988) for this kimberlite. Perovskites from the other four samples yield U–Pb ages of 98 ± 8 to 103 ± 12 Ma. These data confirm that the Somerset Island Province is a part of the widespread Cretaceous kimberlite magmatism in central Canada with age range of 98–113 Ma (Heaman et al., 2004). If all these data are compiled, the weighted age is 100 ± 3 Ma ($n = 12$), which is the best estimation for the emplacement time of kimberlitic magmatism in this area.

5.3. How to obtain meaningful initial isotopic compositions of kimberlite

Isotopic data are vital to understanding the petrogenesis of kimberlites. A common procedure is to obtain isotopic ratios using bulk rocks (e.g., Becker and Le Roex, 2006), as it has been suggested that the high incompatible element contents and rapid ascent through the crust, imply that the effects of contamination by continental crust are minimal (Smith, 1983). However, this conclusion is not supported by leaching experiments, which indicate that a crustal isotopic component is commonly present (Alibert and Albarede, 1988; Malarkey et al., 2008). In addition, it has been argued that, by applying geochemical criteria, whole rocks without any contamination can be selected for analysis (Le Roex et al., 2003) or that a rock can be "cleaned" to exclude later alteration before analysis (Becker and Le Roex, 2006). However, the contaminant is mostly invisible and cannot be removed. Our previous study of the Mengyin kimberlites (China) indicated that the whole-rock samples exhibit a large range of Sr–Nd isotopic variation, although all the analysed samples are "apparently" free of crustal contaminants, thus making it impossible to determine the initial isotopic compositions of the primary magma (Yang et al., 2009).

Clearly, the best method of determining the primary isotopic signature of kimberlite is to analyze a mineral that directly crystallized from the initial magma and remained unaffected by subsequent petrological or weathering processes. Isotopic analyses on multiple grains of perovskite by Heaman (1989), and Malarkey et al. (2008) using the TIMS method, have demonstrated that some discrepancies exist between these and the whole-rock data. Recently, several studies have successfully obtained high quality Sr and Nd isotopic data from kimberlitic perovskites using an excimer laser MC-ICP-MS (Paton et al., 2007a,b; Yang et al., 2009; Woodhead et al., 2009). It is clear that it is essential to analyze perovskite rather than collect whole-rock data if accurate isotopic compositions are to be obtained for the kimberlitic magma.

In terms of technique, thermal ionization mass spectrometry (TIMS) is traditionally used to obtain reliable isotopic compositions. In recent years, micro-sampling, including micro-drilling and/or micro-sawing techniques, have been effectively used for Sr isotopic analyses (Davidson et al., 2007, and references therein). However, the traditional TIMS method involves time consuming complicated chemical separation, and lacks spatial resolution (Davidson et al., 2007). Secondary ionization mass spectrometry (SIMS) has also been used to conduct in situ Sr isotopic analyses (Exley and Jones, 1983), but the precision obtained was much lower than that obtained by TIMS, although this has recently been improved with the new generation of ion microprobes (Weber et al., 2005). Since the advent of inductively-coupled plasma mass spectrometry (ICP-MS), especially the multi-collector (MC) ICP-MS (Halliday et al., 1998), laser ablation has become a powerful method for in situ isotopic measurements, such as for Sr (Davidson et al., 2007; Vroon et al., 2008), Nd (Foster and Vance, 2006; McFarlane and McCulloch, 2007), and Hf (Thirlwall and Walder, 1995), as it can provide rapid, texturally sensitive, high precision isotopic data without the need for chemical preparation of the samples.

Data obtained in this study show that, kimberlitic perovskites exhibit large variations in their trace element contents. With respect to the Lu–Hf system, these perovskites have 0.5–0.9 ppm of Lu and 21–158 ppm of Hf coupled with extremely low $^{176}Lu/^{177}Hf$ ratios of

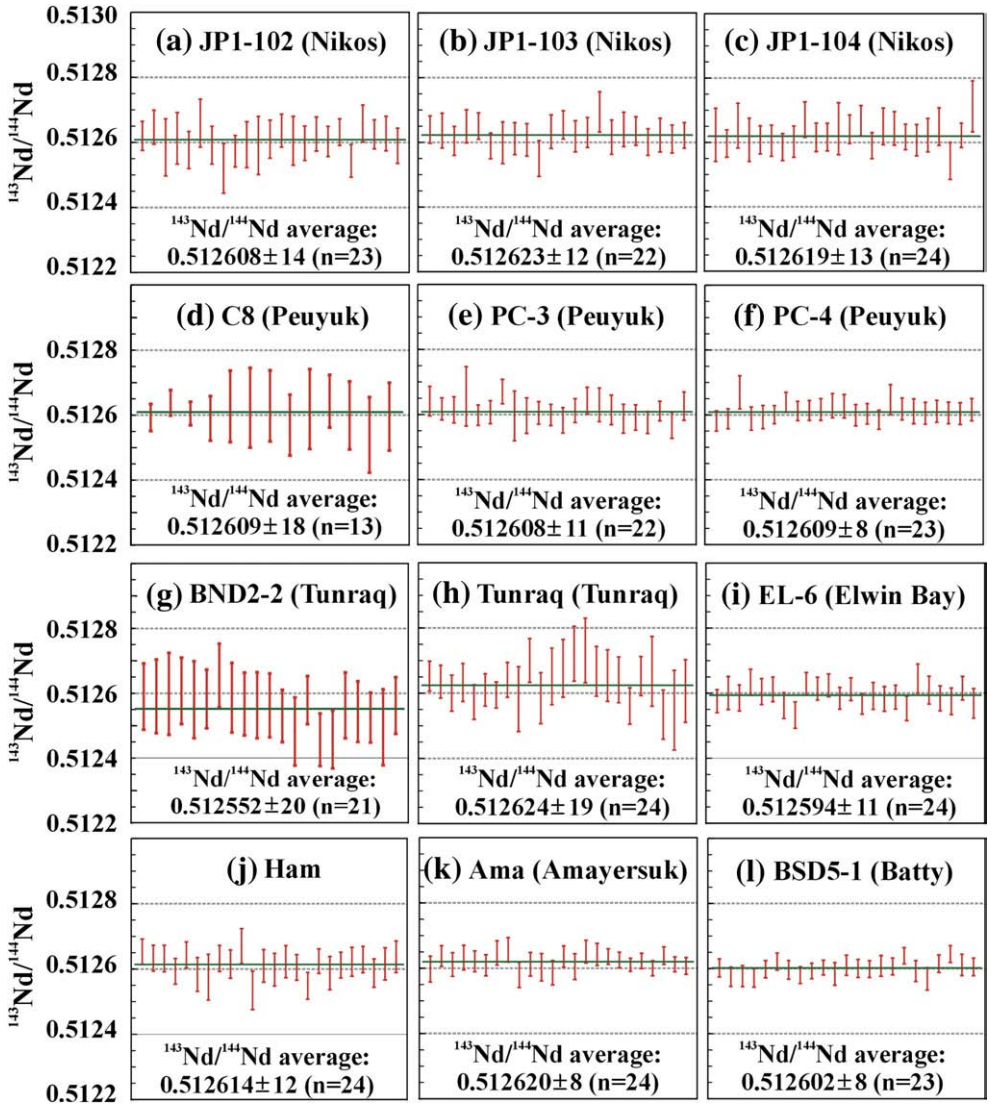

Fig. 9. Nd isotopic compositions of perovskites from kimberlites at Somerset Island, Canada.

Table 2
Nd isotopic data summary of the studied perovskites.

Sample	Location	$^{147}Sm/^{144}Nd$	$2\sigma_m$	$^{143}Nd/^{144}Nd$	$2\sigma_m$	T_{DM} (Ma)	$\varepsilon_{Nd}(t)$	$\varepsilon^{145}{}_{Nd}$
Southern Africa								
W3-680	Wesselton	0.0854	0.0009	0.512662	19	580	1.80	0.34
W2-680a	Wesselton	0.0831	0.0011	0.512634	21	603	1.18	−0.06
W2-680b	Wesselton	0.0827	0.0012	0.512661	19	570	1.76	0.66
W3-680c	Wesselton	0.0876	0.0005	0.512661	24	592	1.66	1.06
BF-18B	Benfontein	0.0779	0.0003	0.512641	14	572	1.42	0.17
OND1-1	Ondermatjie	0.0993	0.0011	0.512427	16	963	2.32	0.32
TP7	Thaba Putsoa	0.0912	0.0014	0.512684	29	581	2.20	0.23
Kao-K1	Kao Gritty	0.0834	0.0010	0.512724	18	499	3.08	−0.57
Somerset Island, Canada								
JP1-102	Nikos	0.0774	0.0003	0.512608	14	607	0.95	−0.95
JP1-103	Nikos	0.0794	0.0005	0.512623	12	599	1.34	−0.55
JP1-104	Nikos	0.0802	0.0004	0.512619	13	607	1.12	−0.63
C8	Peuyuk	0.0692	0.0013	0.512609	18	571	1.24	0.17
PC-03	Peuyuk	0.0708	0.0005	0.512608	11	579	1.09	−0.14
PC-04	Peuyuk	0.0693	0.0004	0.512609	8	572	1.17	−0.37
BND2-2	Tunraq	0.0770	0.0007	0.512552	20	667	−0.17	0.20
Tunraq	Tunraq	0.0783	0.0008	0.512624	19	593	1.31	−0.92
EL-6	Elwin Bay	0.0716	0.0005	0.512594	11	597	0.95	−0.46
Ham	East dike	0.0720	0.0008	0.512614	12	577	1.09	−0.52
Amayersuk	Amayersuk	0.0698	0.0004	0.512620	8	562	1.41	−0.37
BSD5-1	Batty	0.0729	0.0008	0.512602	8	594	1.05	−0.29

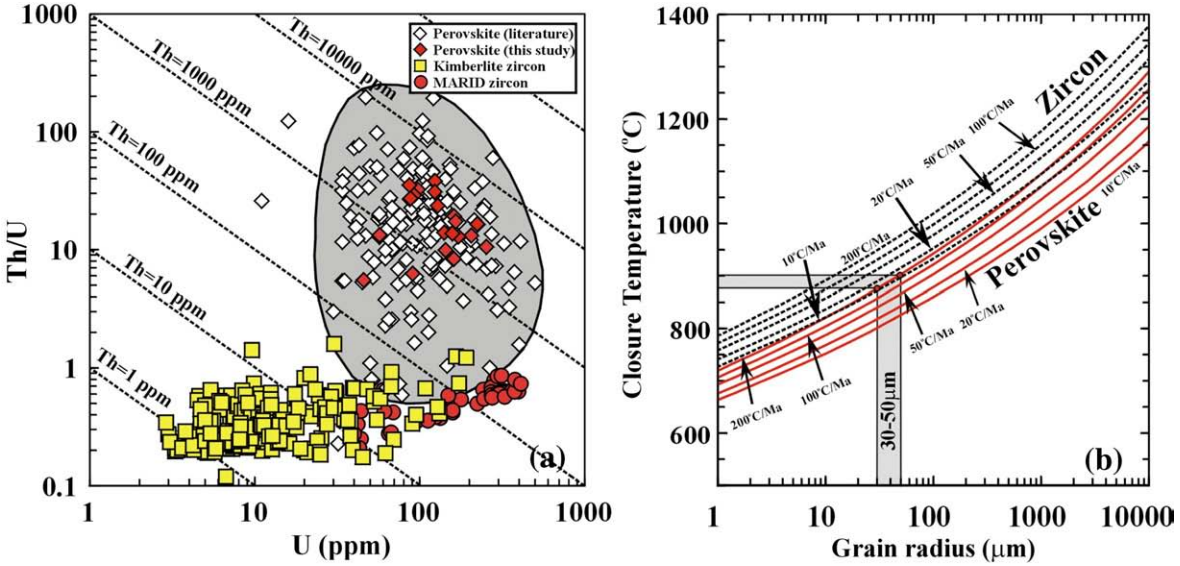

Fig. 10. (a) U and Th concentrations of perovskites and zircons from kimberlites. Data source: Perovskite (literature): Heaman (1989), Smith et al. (1994), Heaman and Kjarsgaard (2000), Heaman et al. (2003, 2004), Kumar et al. (2007); Eccles et al. (2008); Yang et al. (2009); Zurevinski et al. (2008); Kimberlite zircon: Krasnobayev (1980), Kinny et al. (1989), Belousova et al. (1998), Valley et al. (1998), Griffin et al. (2000), Spetsius et al. (2002), Heaman et al. (2003), Zartman and Richardson (2005); MARID zircon: Konzett et al. (1998). (b) Calculation of Pb closure temperature of perovskite following the methods of Dodson (1973) and Zhao and Zheng (2007).

0.0007–0.0046. Although their Hf concentrations are much higher than other minerals, they are not high enough for precise in situ Hf isotopic ratio determination by laser ablation. Therefore, the best method of obtaining precise Hf isotopic compositions remains isotopic dilution using TIMS and/or MC-ICP-MS.

In terms of the Rb–Sr system, the studied perovskites have Rb and Sr concentrations of 0.5–52 and 1097–2411 ppm, with $^{87}Rb/^{86}Sr$ ratios of 0.001–0.082; making it possible to undertake in situ analysis by laser ablation methods. Recent studies have verified the potential of this technique (Paton et al., 2007b; Yang et al., 2009). However, as summarized by Vroon et al. (2008), the isobaric interferences from Kr and Rb are the major obstacles for obtaining accurate data during Sr isotopic measurements. In the case of a mineral containing more than 500 ppm Sr, a spatial resolution (spot size) of approximately 100 μm is required, if a precision of better than 0.0001 is expected. For our studied perovskites in thin sections with Sr concentration of 1000–2000 ppm, a minimum grain-size of 50–60 μm is required for a precision of better than 0.0001. In addition, it has been shown that high accuracy is impossible to obtain when the precision is low (Vroon et al., 2008). Therefore, we abandoned in situ Sr isotopic analyses on the thin sections used in this study, and suggest that mineral separates are required for high precision data as larger grains can be obtained by this method.

Table 3
Perovskite U–Pb age determination by different approaches.

Sample	Common lead ($^{207}Pb/^{206}Pb$)	Lower intercept (Ma) (TW regression)	^{207}Pb correction (Ma) (TW regression)	^{207}Pb correction (Ma) (SK model)	^{204}Pb correction (Ma) (SK model)	Th–Pb age (Ma) (SK model)
W3-680	0.838 ± 0.025	90.0 ± 3.1	90.0 ± 2.0	90.3 ± 2.9		
W2-680a	0.833 ± 0.079	88.6 ± 6.7	88.5 ± 3.0	89.2 ± 2.1		
W2-680b	0.824 ± 0.038	90.5 ± 3.9	90.4 ± 2.2	92.1 ± 2.6		
W2-680b[a]	0.872 ± 0.198	96 ± 12	95.4 ± 7.9	92.3 ± 2.4	90.3 ± 2.9	88.4 ± 1.4
W3-680c	0.852 ± 0.047	89.8 ± 5.1	89.8 ± 2.6	88.8 ± 2.8		
BF-18B	0.836 ± 0.038	87.6 ± 5.0	87.6 ± 2.5	88.3 ± 3.0		
OND1-1	0.796 ± 0.142	515 ± 12	514.8 ± 6.3	520.9 ± 3.6		
TP7	0.842 ± 0.013	89.1 ± 2.1	89.1 ± 1.8	89.0 ± 3.1		
Kao-K1	0.867 ± 0.124	97 ± 13	96.7 ± 6.3	93.7 ± 3.1		
JP1-102	0.835 ± 0.042	101.7 ± 5.8	101.8 ± 3.2	102.6 ± 3.4		
JP1-102[a]	0.984 ± 0.538	110 ± 20	110 ± 14	101.2 ± 2.0	99.5 ± 2.0	103.1 ± 2.5
JP1-103	0.812 ± 0.022	101.7 ± 7.8	101.7 ± 4.3	110.0 ± 6.5		
JP1-104	0.851 ± 0.030	101.1 ± 7.6	100.2 ± 4.2	98.4 ± 5.6		
C8	0.827 ± 0.035	109.1 ± 7.4	108.0 ± 4.5	111.1 ± 5.8		
PC-03	0.824 ± 0.028	97 ± 10	97.3 ± 5.3	103.0 ± 7.4		
PC-03[a]	0.870 ± 0.276	104 ± 29	104 ± 18	99.1 ± 3.6	95.7 ± 5.5	98.4 ± 3.5
PC-04	0.805 ± 0.053	104 ± 14	104.0 ± 7.0	113.1 ± 6.3		
BND2-2	0.821 ± 0.010	92.6 ± 4.4	93.0 ± 3.5	99.5 ± 8.1		
Tunraq	0.813 ± 0.026	100.8 ± 8.6	99.9 ± 5.4	106.2 ± 6.6		
Tunraq[a]	0.992 ± 0.309	112 ± 16	111 ± 10	100.4 ± 3.2	98.8 ± 3.7	99.8 ± 2.4
EL-6	0.837 ± 0.061	104 ± 24	103 ± 12	105 ± 10		
EL-6[a]	0.787 ± 0.131	95 ± 22	95 ± 11	100.3 ± 4.5	99.4 ± 6.5	105.4 ± 4.6
Ham	0.841 ± 0.051	102 ± 20	102 ± 13	102 ± 12		
Ham[a]	0.840 ± 0.120	105 ± 18	104 ± 10	103.0 ± 4.6	97.3 ± 4.8	104.8 ± 4.7
Amayersuk	0.812 ± 0.048	99 ± 17	98.0 ± 8.3	107.5 ± 8.1		
BSD5-1	0.813 ± 0.029	97.5 ± 6.5	97.5 ± 3.5	102.8 ± 4.4		

[a] Data analysed by SIMS, in which, W2-680b is from Li et al. (2010).

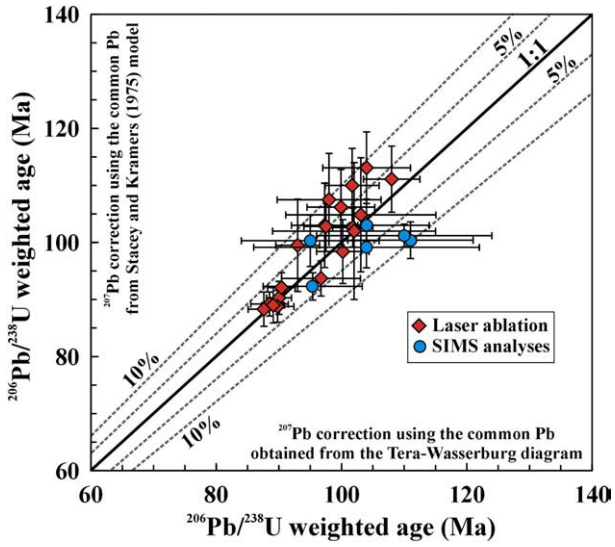

Fig. 11. Comparisons of $^{206}Pb/^{238}U$ weighted ages using ^{207}Pb correction based on different common Pb compositions, upper intercept in the Tera-Wasserburg diagram and the Stacey and Kramers (1975) two-stage model.

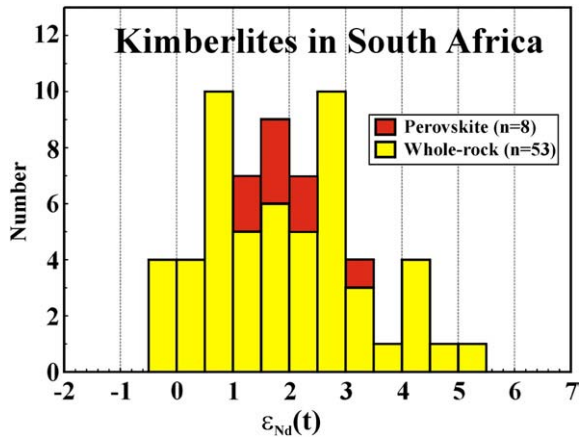

Fig. 12. Histograms comparing the initial Nd isotopic composition of perovskites with whole-rock data for the kimberlites from South Africa. Whole-rock data are from references (Smith, 1983; Heaman, 1989; Nowell et al., 2004; Becker and Le Roex, 2006).

For the Sm–Nd system, the analysed perovskites have Sm and Nd concentrations of 372–1333 and 2295–10,869 ppm, respectively. According to our experiments, only a 20 μm spot size is required for a precision of 0.00005 for the $^{143}Nd/^{144}Nd$ ratio, when the analysed material has a Nd concentration of ~1000 ppm (Yang et al., 2008). Therefore, laser ablation of perovskite can provide reliable Nd isotopic compositions.

In summary, it is impossible in most cases to obtain reliable information for the initial Sr, Hf and Nd isotopic compositions of kimberlites from bulk analyses of whole-rock samples. Groundmass perovskites of euhedral habit without alteration (Fig. 2), can be used to conduct precise Sr–Nd–Hf isotopic measurement as this mineral typically has low Rb and Lu, yet high Sr, Sm, Nd and Hf contents. However, for in situ analyses by laser ablation, the Hf concentrations of 21–158 ppm make it impossible to obtain Hf isotopic compositions with high precision. In situ Sr isotopic analysis is applicable in many cases, but the small grain-size of many kimberlite perovskites makes this method ineffective for use with thin sections. According to this study, in situ Nd isotopic analyses are easier to obtain relative to the Sr and Hf isotopic data.

5.4. Nd isotopic constraints on the source of kimberlites

All kimberlites studied in this work are archetypal kimberlites (Mitchell, 1995, 2006). Their genesis remains controversial and diverse conflicting hypotheses have been advanced with respect to the character and location of their sources. These include: depleted mantle within the lithosphere (Heaman, 1989; Becker and Le Roex, 2006); ancient and isolated deeply subducted oceanic basalt beneath the lithosphere (Nowell et al., 2004); and the convective asthenospheric mantle (Mitchell, 1986, 1995). A key aspect of the controversy is whether kimberlites are derived from the lithosphere or the asthenosphere. Geochemical studies have established that lithospheric mantle is highly heterogeneous with regard to age and metasomatism of the source material (Pearson, 1999; Pearson et al., 2003; Carlson et al., 2005; Davies, 2007). Particularly, the metasomatism results in a large range of Sr–Nd–Hf isotopic compositional variations (Fraser et al., 1985; Pearson et al., 2003; Mitchell, 2006; Simon et al., 2007). However, the fact that kimberlites exhibit identical Sr–Nd geochemical features whether they are emplaced within a craton or associated accreted mobile belts (Mitchell, 1995), strongly indicates that kimberlites are derived from sources unrelated to the overlying lithosphere.

If kimberlites are derived from asthenospheric sources, a further question to be answered is whether this source is located in the highly depleted upper mantle or weakly-depleted lower mantle. The initial Sr ratios from whole-rock kimberlites in southern African range from 0.7032 to 0.7077 (Smith, 1983; Heaman, 1989; Nowell et al., 2004; Becker and Le Roex, 2006). However, the perovskites from the same kimberlite samples show a narrow range of 0.704–0.705 (Woodhead et al., 2009). In terms of Nd isotopes, the calculated $\varepsilon_{Nd}(t)$ values from whole rocks are −0.5 to +5.1 (Fig. 12, Smith, 1983; Heaman, 1989; Nowell et al., 2004; Becker and Le Roex, 2006), whereas the perovskites have much narrower range of +1.2 to +3.1. For Somerset Island, five kimberlite whole-rock samples from Nikos yield $\varepsilon_{Nd}(t)$ values of +0.88 to+1.34 (Schmidberger et al., 2001), comparable to our in situ analyses from perovskites (+0.74 to +1.27 with one exception of −0.17). However, Heaman (1989) reported an $\varepsilon_{Nd}(t)$ value of +5.6 for the perovskite from Ham kimberlite, much higher than our value of +1.12 from the same intrusion. Regardless, our $\varepsilon_{Nd}(t)$ values obtained from perovskites are much lower than +10, the typical value of the depleted asthenospheric mantle (Salters and Stracke, 2004). The Sr–Nd isotopic data indicate that the primary melt of kimberlite is isotopically primitive. On this basis, it is proposed that kimberlite might be derived from the lower mantle. This conclusion is also supported by other direct evidence suggesting that kimberlites might be derived from the lower mantle or mantle plumes originating from the core–mantle boundary (Ringwood et al., 1992; Haggerty, 1994, 1999; Bizzarro et al., 2002; Nowell et al., 2004). In particular diamonds from kimberlites can contain mineral inclusions indicative of derivation from the deep mantle (Harte and Harris, 1994; Gasparik, 2000; Kerschhofer et al., 2000; Stachel et al., 2000a,b; Kaminsky et al., 2001; Tachibana et al., 2006).

6. Conclusions

In situ U–Pb age determination and Nd isotopic analyses of perovskite from kimberlites in southern Africa and Somerset Island, Canada lead to the following conclusions:

1) In situ U–Pb age determination of perovskites indicates that the kimberlites in southern Africa were mostly emplaced during the Cretaceous with ages of 88 ± 3 to 97 ± 6 Ma. The presence of an Early Paleozoic (515 ± 6 Ma) kimberlite at Ondermatjie has been identified. Samples from Somerset Island yield ages of 93 to 108 Ma, slightly older than those in southern Africa, but contemporaneous with other Cretaceous kimberlite magmatism in Canada;

2) Although whole-rock analyses of the kimberlites from southern Africa have a large range of $\varepsilon_{Nd}(t)$ values of −0.5 to +5.1, the analysed perovskites from southern Africa show a more limited range of +1.2 to +3.1, with those from the Somerset Island giving +0.95 to +1.41, and much lower than the typical value of depleted asthenospheric mantle, suggesting that kimberlites are probably derived from the lower mantle;
3) Rapid in situ U–Pb and Nd isotopic analyses of perovskites by laser ablation can provide important constraints on the emplacement age and source regions of kimberlites.

Acknowledgments

We are grateful to Jin-Feng Sun and Wei-Qiang Ji for their help during data acquisition. Zi-Fu Zhao is thanked for the calculation of Pb closure temperature. Chad Paton reviewed an original version of this paper and provided numerous suggestions. Thoughtful and constructive comments by Chris McFarlane and an anonymous referee have substantially improved the manuscript. This study was supported by the Natural Science Foundation of China (grants 40634019 and 40773008) and the Chinese Academy of Sciences. RHM acknowledges financial and logistical support from the Natural Sciences and Engineering Research Council of Canada and De Beers Consolidated Mines Ltd, respectively. Jennifer Pell is thanked for samples of the Nikos kimberlite.

Appendix A. Supplementary data

Supplementary data associated with this article can be found, in the online version, at doi:10.1016/j.lithos.2009.12.010.

References

Alibert, C., Albarede, F., 1988. Relationships between mineralogical, chemical, and isotopic properities of some North America kimberlites. Journal of Geophysical Research 93, 7643–7671.
Allsopp, H.L., Bristow, J.W., Smith, C.B., Brown, R., Gleadow, A.J.W., Kramers, J.D., Garvie, O.G., 1989. A summary of radiometric dating methods applicable to kimberlite and related rocks. In: Ross, J. (Ed.), Proceedings of the 4th International Kimberlite Conference, v. 1, Kimberlites and related rocks: their composition, occurrence, origin and emplacement. Geological Society of Australia Special Publication, vol. 14. Blackwell Scientific Publications, Oxford, pp. 343–357.
Batumike, J.M., Griffin, W.L., Belousova, E.A., Pearson, N.J., O'Reilly, S.Y., Shee, S.R., 2008. LAM–ICPMS U–Pb dating of kimberlitic perovskite: Eocene-Oligocene kimberlites from the Kundelungu Plateau, D. R. Congo. Earth and Planetary Science Letters 267, 609–619.
Becker, M., Le Roex, A.P., 2006. Geochemistry of South African on- and off-craton, Group I and Group II kimberlites: petrogenesis and source region evolution. Journal of Petrology 47, 673–703.
Becker, M., Le Roex, A.P., Class, C., 2007. Geochemistry and petrogenesis of South African transitional kimberlites located on and off the Kaapvaal Craton. South African Journal of Geology 110, 631–646.
Belousova, E.A., Griffin, W.L., Pearson, N.J., 1998. Trace element composition and cathodoluminescence properties of kimberlitic zircons from southern Africa. Mineralogical Magazine 62, 355–366.
Belousova, E.A., Griffin, W.L., Shee, S.R., Jackson, S.E., O'Reilly, S.Y., 2001. Two age populations of zircons from the Timber Creek kimberlites, Northern territory, Australia as determined by laser-ablation ICPMS analysis. Australian Journal of Earth Sciences 48, 757–766.
Bizzarro, M., Simonetti, A., Stevenson, R.K., David, J., 2002. Hf isotope evidence for a hidden mantle reservoir. Geology 30, 771–774.
Carlson, R.W., Boyd, F.R., Shirey, S.B., Janney, P.E., Grove, T.L., Bowring, S.A., Schmitz, M.D., Dann, J.C., Bell, D.R., Gurney, J.J., Richardson, S.H., Tredoux, M., Menzies, A.H., Pearson, D.G., Hart, R.J., Wilson, A.H., Moser, D., 2000. Continental growth, preservation, and modification in southern Africa. GSA Today 10, 1–7.
Carlson, R.W., Pearson, D.G., James, D.E., 2005. Physical, chemical, and chronological characteristics of continental mantle. Review of Geophysics 43 2004RG000156.
Chakhmouradian, A.R., Mitchell, R.H., 2001a. Occurrence, alteration patterns and compositional variation of perovskite in kimberlites. Canadian Mineralogist 38, 975–994.
Chakhmouradian, A.R., Mitchell, R.H., 2001b. Three compositional varieties of perovskite from kimberlites of the Lac de Gras field (Northwest Territories, Canada). Mineralgical Magazine 65, 133–148.
Chipley, D., Polito, P.A., Kyser, T.K., 2007. Measurement of U–Pb ages of uraninite and davidite by laser ablation–HR–ICP–MS. American Mineralogist 92, 1925–1935.
Clement, C.R., 1973. Kimberlites from the Kao pipe, Lesotho. In: Nixon, P.H. (Ed.), Lesotho Kimberlites. Lesotho National Development Corporation, Maseru, pp. 110–121.
Corfu, F., Dahlgren, S., 2008. Perovskite U–Pb ages and the Pb isotopic composition of alkaline volcanism initiating the Permo-Carboniferous Olso Rift. Earth and Planetary Science Letters 265, 256–269.
Cox, R.A., Wilton, D.H.C., 2006. U–Pb dating of perovskite by LA–ICP–MS: an example from the Oka carbonatite, Quebec, Canada. Chemical Geology 235, 21–32.
Cox, R.A., Wilton, D.H.C., Kosler, J., 2003. Laser-ablation U–Th–Pb in situ dating of zircon and allanite: an example from the October Harbour granite, central Coastal Labrador, Canada. Canadian Mineralogist 41, 273–291.
Davidson, J.P., Morgan, D.J., Charlier, B.L.A., Harlou, R., Hora, J.M., 2007. Microsampling and isotopic analysis of igneous rocks: implications for the study of magmatic systems. Annual Review of Earth and Planetary Sciences 35, 273–311.
Davies, G.R., 2007. The origin and evolution of the Kaapvaal cratonic lithospheric mantle. Journal of Petrology 48, 589–625.
Davis, G.L., Krogh, T.E., Erlank, A.J., 1976. The ages of zircons from kimberlites from South Africa. Year Book–Carnegie Institution of Washington, vol. 75, pp. 821–824.
Dodson, M.H., 1973. Closure temperature in cooling geochronological and petrological systems. Contributions to Mineralogy and Petrology 40, 259–274.
Dubois, J.C., Retali, G., Cesario, J., 1992. Isotopic analysis of rare earth elements by total vaporization of samples in thermal ionization mass spectrometry. International Journal of Mass Spectrometry and Ion Processes 120, 163–177.
Eccles, D.R., Creaser, R.A., Heaman, L.M., Ward, J., 2008. Rb–Sr and U–Pb geochronology and setting of the Buffalo Head Hills kimberlite field, northern Alberta. Canadian Journal of Earth Sciences 45, 513–529.
Exley, R.A., Jones, A.P., 1983. $^{87}Sr/^{86}Sr$ in kimberlite carbonates by ion microprobe: hydrothermal alteration, crustal contamination and relation to carbonatite. Contributions Mineralogy and Petrology 83, 288–292.
Foster, G.L., Carter, A., 2007. Insights into the patterns and locations of erosion in the Himalaya — a combined fission-track and in situ Sm–Nd isotopic study of detrital apatite. Earth and Planetary Science Letters 257, 407–418.
Foster, G.L., Vance, D., 2006. In situ Nd isotopic analysis of geological materials by laser ablation MC–ICP–MS. Journal of Analytical Atomic Spectrometry 21, 288–296.
Fraser, K.J., Hawkesworth, C.J., Erlank, A.J., Mitchell, R.H., Scott-Smith, B.H., 1985. Sr, Nd and Pb isotope and minor element geochemistry of lamproites and kimberlites. Earth and Planetary Science Letters 76, 57–70.
Frei, D., Hutchison, M.T., Gerdes, A., Heaman, L.M., 2008. Common-lead corrected U–Pb dating of perovskite by laser ablation-magnetic sectorfield ICP–MS. 9th International Kimberlite Conference Extended Abstract, p. 00216.
Gasparik, T., 2000. Evidence for the transition zone origin of some [Mg, Fe]O inclusions in diamond. Earth and Planetary Science Letters 183, 1–5.
Gregory, C.J., Rubatto, D., Allen, C.M., Williams, I.S., Hermann, J., Ireland, T., 2007. Allanite micro-geochronology: a LA–ICP–MS and SHRIMP U–Th–Pb study. Chemical Geology 245, 162–182.
Griffin, W.L., Pearson, N.J., Belousova, E., Jackson, S.E., van Achterbergh, E., O'Reilly, S.Y., Shee, S.R., 2000. The Hf isotope composition of cratonic mantle: LAM–MC–ICPMS analysis of zircon megacrysts in kimberlites. Geochimica et Cosmochimica Acta 64, 133–147.
Guillong, M., Horn, I., Günther, D., 2003. A comparison of 266 nm, 213 nm and 193 nm produced from a single solid state Nd:YAG laser for laser ablation ICP–MS. Journal of Analytical and Atomic Spectrometry 18, 1224–1230.
Haggerty, S.E., 1994. Superkimberlites: a geodynamic window to the Earth's core. Earth and Planetary Science Letters 122, 57–69.
Haggerty, S.E., 1999. A diamond trilogy: superplumes, supercontinents, and supernovae. Science 285, 851–860.
Halliday, A.N., Lee, D.-C., Christensen, J.N., Rehkamper, M., Yi, W., Luo, X., Hall, C.M., Ballentine, C.J., Pettke, T., Stirling, C., 1998. Applications of multiple collector—ICPMS to cosmochemistry, geochemistry, and paleoceanography. Geochimica et Cosmochimica Acta 62, 919–940.
Harte, B., Harris, J.W., 1994. Lower mantle mineral associations preserved in diamonds. Mineralogical Magazine 58A, 384–385.
Heaman, L.M., 1989. The nature of the subcontinental mantle from Sr–Nd–Pb isotopic studies on kimberlitic perovskite. Earth and Planetary Science Letters 92, 323–334.
Heaman, L.M., Kjarsgaard, B.A., 2000. Timing of eastern North American kimberlite magmatism: continental extension of the Great Meteor hotspot track? Earth and Planetary Science Letters 178, 253–268.
Heaman, L.M., Kjarsgaard, B.A., Creaser, R.A., 2003. The timing of kimberlite magmatism in North America: implications for global kimberlite genesis and diamond exploration. Lithos 71, 153–184.
Heaman, L.M., Kjarsgaard, B.A., Creaser, R.A., 2004. The temporal evolution of North American kimberlites. Lithos 76, 377–397.
Horn, I., Rudnick, R.L., McDonough, W.F., 2000. Precise elemental and isotope ratio determination by simultaneous solution nebulization and laser ablation–ICP–MS: application to U–Pb geochronology. Chemical Geology 167, 405–425.
Horstwood, M.S.A., Foster, G.L., Parrish, R.R., Noble, S.R., Nowell, G.M., 2003. Common-Pb corrected in situ U–Pb accessory mineral geochronology by LA–MC–ICP–MS. Journal of Analytical Atomic Spectrometry 18, 837–846.
Irvine, G.J., Pearson, D.G., Kjarsgaard, B.A., Carlson, R.W., Kopylova, M.G., Dreibus, G., 2003. A Re–Os isotope and PGE study of kimberlite-derived peridotite xenoliths from Somerset Island and a comparison to the Slave and Kaapvaal cratons. Lithos 71, 461–488.
Isnard, H., Brennetot, R., Caussignac, C., Caussignac, N., Chartier, F., 2005. Investigations for determination of Gd and Sm isotopic compositions in spent nuclear fuels samples by MC ICPMS. International Journal of Mass Spectrometry 246, 66–73.
Jelsma, H.A., de Wit, M.J., Thiart, C., Dirks, P.H.G.M., Viola, G., Basson, I.J., Anckar, E., 2004. Preferential distribution along transcontinental corridors of kimberlites and related rocks of southern Africa. South African Journal of Geology 107, 301–324.
Jones, A.P., Wyllie, P.J., 1984. Minor elements in perovskite from kimberlites and distribution of the rare earth elements: an electron probe study. Earth and Planetary Science Letters 69, 128–140.
Kaminsky, F.V., Zakharchenko, O.D., Davies, R., Griffin, W.L., Khachatryan-Blinova, G.K., Shiryaev, A.A., 2001. Superdeep diamonds from the Juina area, Mato Grosso State, Brazil. Contributions to Mineralogy and Petrology 140, 734–753.

Kerschhofer, L., Schärer, U., Deutsch, A., 2000. Evidence for crystals from the lower mantle: baddeleyite megacrysts of the Mbuji Mayi kimberlite. Earth and Planetary Science Letters 179, 219–225.
Kinny, P.D., Meyer, H.O.A., 1994. Zircons from the mantle: a new way to date old diamonds. Journal of Geology 102, 475–481.
Kinny, P.D., Compston, W., Bristow, J.W., Williams, I.S., 1989. Archean mantle xenocrysts in a Permian kimberlite: two generations of kimberlitic zircon in Jwaneng DK2, southern Botswana. In: Ross, J. (Ed.), Kimberlites and Related Rocks: Their mantle/crust setting, diamonds and diamond exploration. : Geological Society of Australia Special Publication, vol. 14,(2). Blackwell Scientific Publications, Oxford, pp. 833–842.
Kinny, P.D., Griffin, B.J., Heaman, L.M., Brakhfogel, F.F., Spetsius, Z.V., 1997. SHRIMP U–Pb ages of perovskite from Yakutian kimberlites. Russian Geology and Geophysics 38, 97–105.
Konzett, J., Armstrong, R.A., Sweeney, R.J., Compston, W., 1998. The timing of MARID metasomatism in the Kaapvaal mantle: an ion probe study of zircons from MARID xenoliths. Earth and Planetary Science Letters 160, 133–145.
Košler, J., Wiedenbeck, M., Wirth, R., Hovorka, J., Sylvester, P., Mıkova, J., 2005. Chemical and phase composition of particles produced by laser ablation of silicate glass and zircon—implications for elemental fractionation during ICP–MS analysis. Journal of Analytical Atomic Spectrometry 20, 402–409.
Kramers, J.D., Smith, C.B., 1983. A feasibility study of U–Pb and Pb–Pb dating of kimberlites using groundmass mineral fractions and whole-rock samples. Chemical Geology 1, 23–38.
Krasnobayev, A.A., 1980. Mineralogical and geochemical features of zircons from kimberlites and problem pf their origin. International Geology Review 22, 1199–1209.
Kumar, A., Heaman, L.M., Manikyamba, C., 2007. Mesoproterozoic kimberlites in south India: a possible link to 1.1 Ga global magmatism. Precambrian Research 154, 192–204.
Le Roex, A.P., Bell, D.R., Davis, P., 2003. Petrogenesis of Group I kimberlites from Kimberley, South Africa: evidence from bulk-rock geochemistry. Journal of Petrology 44, 2261–2286.
Li, X.H., Liu, Y., Li, Q.L., Guo, C.H., Chamberlain, K.R., 2009. Precise determination of Phanerozoic zircon Pb/Pb age by multi-collector SIMS without external standardization. Geochemistry, Geophysics, Geosystem. doi:10.1029/2009GC00 2400.
Li, Q.L., Li, X.H., Liu, Y., Wu, F.Y., Yang, J.H., Griffin, W.L., Mitchell, R.H., 2010. Precise U–Pb and Th–Pb age determination of kimberlitic perovskites secondary ion mass spectrometry. Chemical Geology. doi:10.1016/j.chemgeo.2009.10.014.
Ludwig, K.R., 2003. ISOPLOT 3.0—a geochronological toolkit for Microsoft Excel. Berkeley Geochronology Center Special Publication, No. 4, p. 70.
Malarkey, J., Pearson, D.G., Nowell, G.M., Davidson, J.P., Kjarsgaard, B., Ottley, C.J., Mitchell, R.H., Kopylova, M., 2008. Constraining the crust and mantle contributions to kimberlite. 9th International Kimberlite Conference Extended Abstract, p. 00145.
Masuda, A., Nakamura, N., Tanaka, T., 1973. Fine structures of mutually normalized rare-earth patterns of chondrites. Geochimica et Cosmochimica Acta 37, 239–248.
McFarlane, C.R.M., McCulloch, M.T., 2007. Coupling of in-situ Sm–Nd systematics and U–Pb dating of monazite and allanite with applications to crustal evolution studies. Chemical Geology 245, 45–60.
Melluso, L., Lustrino, M., Ruberti, E., Brotzu, P., Gomes, C.B., Morbidelli, L., Morra, V., Svisero, D.P., D'Amelio, F., 2008. Major- and trace-element composition of olivine, perovskite, clinopyroxene, Cr–Fe–Ti oxides, phlogopite and host kamafugites and kimberlites, Alta Paranaiba, Brazil. Canadian Mineralogist 46, 19–40.
Mitchell, R.H., 1972. Composition of perovskite in kimberlite. American Mineralogist 57, 1748–1753.
Mitchell, R.H., 1975. Geology, magnetic expression, and structural control of the central Somerset Island kimberlites. Canadian Journal of Earth Sciences 12, 757–764.
Mitchell, R.H., 1977. Ultramafic xenoliths from the Elwin Bay kimberlite — the first Canadian paleogeotherm. Canadian Journal of Earth Science 14, 1202–1210.
Mitchell, R.H., 1979. Mineralogy of the Tunraq kimberlite, Somerset Island, N.W.T., Canada. In: Boyd, F.R., Meyer, H.O.A. (Eds.), Kimberlites, diatremes and diamonds: their geology and geochemistry. Proceedings of the Second International Kimberlite Conference, American Geophysical Union Washington, vol. 1, pp. 161–171.
Mitchell, R.H., 1986. Kimberlites: mineralogy, geochemistry, and petrology. Plenum Press, New York. 442p.
Mitchell, R.H., 1995. Kimberlites, orangeites, and related rocks. Plenum Press, New York. 410 pp.
Mitchell, R.H., 2004. Experimental studies at 5–12 GPa of the Ondermatjie hypabyssal kimberlite. Lithos 76, 551–564.
Mitchell, R.H., 2006. Potassic magmas derived from metasomatized lithospheric mantle: nomenclature and relevance to explanation for diamond bearing rocks. Journal Geological Society of India 67, 317–327.
Mitchell, R.H., Fritz, P., 1973. Kimberlite from Somerset Island, District of Franklin, N.W.T., Canada. Canadian Journal of Earth Sciences 10, 384–393.
Mitchell, R.H., Meyer, H.O.A., 1980. Mineralogy of micaceous kimberlite from the Jos dike, Somerset Island, N.W.T., Canada. Canndian Mineralgist 18, 241–250.
Mitchell, R.H., Reed, S.J., 1988. Ion microprobe determination of rare earth elements in perovskite from kimberlites and alnoites. Mineralogical Magazine 52, 331–339.
Mitchell, R.H., Kjarsgaard, B.A., McBride, J., 2009. Mineralogy of juvenile lapilli in Fort a la Corne pyroclastic kimberlites. Geological Association of Canada – Mineralogical Association of Canada – American Geophysical Union; Joint meeting abstract, Toronto, Ontario.
Nowell, G.M., Pearson, D.G., Bell, D.R., Carlson, R.W., Smith, C.B., Kempton, P.D., Noble, S.R., 2004. Hf isotope systematics of kimberlites and their megacrysts: new constraints on their source regions. Journal of Petrology 45, 1583–1612.
Paton, C., Hergt, J.M., Phillips, D., Woodhead, J.D., Shee, S.R., 2007a. New insights into the genesis of Indian kimberlites from the Dharwar Craton via in situ Sr isotope analysis of groundmass perovskite. Geology 35, 1011–1014.
Paton, C., Woodhead, J., Hergt, J., Phillips, D., Shee, S., 2007b. Sr-isotope analysis of kimberlitic groundmass perovskite via LA-MCICPMS. Geostandards and Geoanalytical Research 31, 321–330.
Pearson, D.G., 1999. Evolution of cratonic lithospheric mantle: an isotopic perspective. In: Fei, Y., Bettka, C.M., Mysen, B.O. (Eds.), Mantle petrology: field observations and high pressure experimentation: Geochemical Society Special Publications, vol. 6, pp. 57–78.
Pearson, D.G., Canil, D., Shirey, S.B., 2003. Mantle samples included in volcanic rocks: xenoliths and diamonds. In: Carlson, R.W. (Ed.), The Mantle and Core. Treatise on Geochemistry, vol. 2, pp. 171–276.
Phillips, D., Kiviets, G.B., Barton, E.S., Smith, C.B., Viljoen, K.S., Fourie, L.F., 1999. $^{40}Ar/^{39}Ar$ dating of kimberlites and related rocks: problems and solution. In: Gurney, J.J., Gurney, J.L., Pascoe, M.D., Richardson, S.H. (Eds.), Proceedings of the 7th International Kimberlite Conference, Cape Town, South Africa, vol. 2, pp. 677–688.
Ringwood, A.E., Kesson, S.E., Hibberson, W., Ware, N., 1992. Origin of kimberlites and related magmas. Earth and Planetary Science Letters 113, 521–538.
Rocholl, A., Dulski, P., Raczek, I., 2000. New ID–TIMS, ICP–MS and SIMS data on the trace element composition and homogeneity of NIST certified reference material SRM 610–611. Geostandards Newsletter 24, 261–274.
Salters, V.J.M., Stracke, A., 2004. Composition of the depleted mantle. Geochemistry Geophysics Geosystems 5, Q05004. doi:10.1029/2003GC000597.
Schmidberger, S.S., Francis, D., 1999. Nature of the mantle roots beneath the North American craton: mantle xenolith evidence from Somerset Island kimberlites. Lithos 48, 195–216.
Schmidberger, S.S., Francis, D., 2001. Constraints on the trace element composition of the Archean mantle root beneath Somerset Island, Arctic Canada. Journal of Petrology 42, 1095–1117.
Schmidberger, S.S., Simonetti, A., Francis, D., 2001. Sr–Nd–Pb isotope systematics of mantle xenoliths from Somerset Island kimberlites: evidence for lithosphere stratification beneath Arctic Canada. Geochimica et Cosmochimica Acta 65, 4243–4255.
Schmidberger, S.S., Simonetti, A., Francis, D., Gariepy, C., 2002. Probing Archean lithosphere using the Lu–Hf isotope systematics of peridotite xenoliths from Somerset Island kimberlites, Canada. Earth and Planetary Science Letters 197, 245–259.
Schmidberger, S.S., Simonetti, A., Francis, D., 2003. Small-scale Sr isotope investigation of clinopyroxenes from peridotite xenoliths by laser ablation MC–ICP–MS—implications for mantle metasomatism. Chemical Geology 199, 317–329.
Shee, S.R., Bristow, J.W., Bell, D.R., Smith, C.B., Allsopp, H.L., Shee, P.B., 1989. The petrology of kimberlites, related rocks and associated mantle xenoliths from the Kuruman Province, South Africa. In: Ross, J. (Ed.), Proceedings of the 4th International Kimberlite Conference, v. 1, Kimberlites and related rocks: their composition, occurrence, origin and emplacement. : Geological Society of Australia Special Publication, vol. 14. Blackwell Scientific Publications, Oxford, pp. 60–82.
Simon, N.S.C., Carlson, R.W., Pearson, D.G., Davies, G.R., 2007. The origin and evolution of the Kaapvaal cratonic lithospheric mantle. Journal of Petrology 48, 589–625.
Skinner, E.M.W., 1989. Contrasting group I and group II kimberlite petrology: towards a genetic model for kimberlites. In: Ross, J. (Ed.), Kimberlites and related rocks: their composition, occurrence, origin and emplacement. : Geological Society of Australia. Special Publication, vol. 14,(1). Blackwell Sci. Publ, pp. 528–544.
Smith, C.B., 1983. Pb, Sr and Nd isotopic evidence for sources of southern African Cretaceous kimberlites. Nature 304, 51–54.
Smith, C.B., Gurney, J.J., Skinner, E.M.W., Clement, C.R., Ebrahim, N., 1985. Geochemical character of southern African kimberlites: a new approach based on isotopic constraints. Transactions of the Geological Society of South Africa 88, 267–280.
Smith, C.B., Colgan, E.A., Hawthorne, J.B., Hutchinson, G., 1988. Emplacement age of the Cross kimberlite, southesastern British Columbia, by the Rb–Sr phlogopite method. Canadian Journal of Earth Sciences 25, 790–793.
Smith, C.B., Allsopp, H.L., Gravie, O.G., Kramers, J.D., Jackson, P.F.S., Clement, C.R., 1989. Note on the U–Pb perovskite method for dating kimberlites: examples from the Wesselton and De Beers mines, South Africa, and Somerset Island, Canada. Chemical Geology 79, 137–145.
Smith, C.B., Clark, T.C., Barton, E.A., Bristow, J.W., 1994. Emplacement ages of kimberlite occurrences in the Prieska region, southwest border of the Kaapvaal Craton, South Africa. Chemical Geology 113, 149–169.
Spetsius, Z.V., Belousova, E.A., Griffin, W.L., O'Reilly, S.Y., Pearson, N.J., 2002. Archean sulfide inclusions in Paleozoic zircon megacrysts from the Mir kimberlite, Yakutia: implications for the dating of diamonds. Earth and Planetary Science Letters 199, 111–116.
Stacey, J.S., Kramers, J.D., 1975. Approximation of terrestrial lead isotope evolution by a two stages model. Earth and Planetary Science Letters 26, 207–221.
Stachel, T., Brey, G.P., Harris, J.W., 2000a. Kankan diamonds (Guinea) I: From the lithosphere down to the transition zone. Contributions to Mineralogy and Petrology 140, 1–15.
Stachel, T., Harris, J.W., Brey, G.P., Joswig, W., 2000b. Kankan diamonds (Guinea) II: Lower mantle inclusion parageneses. Contributions to Mineralogy and Petrology 140, 16–27.
Storey, C.D., Jeffries, T.E., Smith, M., 2006. Common lead-corrected laser ablation ICP–MS U–Pb systematics and geochronology of titanite. Chemical Geology 227, 37–52.
Tachibana, Y., Kaneoka, I., Gaffney, A., Upton, B., 2006. Ocean-island basalt-like source of kimberlite magmas from West Greenland revealed by high $^{3}He/^{4}He$ ratios. Geology 34, 273–276.
Thirlwall, M.F., Walder, A.J., 1995. In situ hafnium isotope ratio analysis of zircon by inductively coupled plasma multiple collector mass spectrometry. Chemical Geology 122, 241–247.
Valley, J.W., Kinny, P.D., Schulze, D.J., Spicuzza, M.J., 1998. Zircon megacrysts from kimberlite: oxygen isotope variability among mantle melts. Contributions to Mineralogy and Petrology 133, 1–11.
Vance, D., Thirlwall, M., 2002. An assessment of mass discrimination in MC–ICPMS using Nd isotopes. Chemical Geology 185, 227–240.

Vroon, P.Z., van der Wagt, B., Koornneef, J.M., Davies, G.R., 2008. Problems in obtaining precise and accurate Sr isotope analysis from geological materials using laser ablation MC–ICPMS. Analytical and Bioanalytical Chemistry 390, 465–476.

Vry, J.K., Baker, J.A., 2006. LA–MC–ICPMS Pb–Pb dating of rutile from slowly cooled granulites: confirmation of the high closure temperature for Pb diffusion in rutile. Geochimica Cosmochimica Acta 70, 1807–1820.

Wasserburg, G.J., Jacobsen, S.B., DePaolo, D.J., McCulloch, M.T., Wen, T., 1981. Precise determination of Sm/Nd ratios, Sm and Nd isotopic abundances in standard solutions. Geochimica et Cosmochimica Acta 45, 2311–2323.

Weber, P.K., Bacon, C.R., Hutcheon, I.D., Ingram, B.L., Wooden, J.L., 2005. Ion microprobe measurement of strontium isotopes in calcium carbonate with application to salmon otoliths. Geochimica et Cosmochimica Acta 69, 1225–1239.

Williams, I.S., 1998. U–Th–Pb geochronology by ion microprobe. In: McKibben, M.A., ShanksIII III, W.C., Ridley, W.I. (Eds.), Applications of microanalytical techniques to understanding mineralizing processes: Reviews in Economic Geology, vol. 7, pp. 1–35.

Woodhead, J.D., Hergt, J.M., 2001. Strontium, Neodymium and Lead isotope analyses of NIST glass certified reference materials: SRM 610, 612, 614. Geostandards Newsletter 25, 261–266.

Woodhead, J.D., Hergt, J.M., Phillips, D., Paton, C., 2009. African kimberlites revisited: in situ Sr-isotope analysis of groundmass perovskite. Lithos 112S, 311–317.

Wu, F.Y., Yang, Y.H., Xie, L.W., Yang, J.H., Xu, P., 2006. Hf isotopic compositions of the standard zircons and baddeleyites used in U–Pb geochronology. Chemical Geology 234, 105–126.

Xie, L.W., Zhang, Y.B., Zhang, H.H., Sun, J.F., Wu, F.Y., 2008. In situ simultaneous determination of trace elements, U–Pb and Lu–Hf isotopes in zircon and baddeleyite. Chinese Science Bulletin 53, 1565–1573.

Yang, Y.H., Zhang, H.F., Xie, L.W., Wu, F.Y., 2007. Accurate measurement of neodymium isotopic composition using Neptune multiple collector inductively coupled plasma mass spectrometry (in Chinese with English abstract). Chinese Journal of Analytical Chemistry 35, 71–74.

Yang, Y.H., Sun, J.F., Xie, L.W., Fan, H.R., Wu, F.Y., 2008. In situ Nd isotopic measurement of geological samples by laser ablation. Chinese Science Bulletin 53, 1062–1070.

Yang, Y.H., Wu, F.Y., Wilde, S.A., Xliu, X.M., Zhang, Y.B., Xie, L.W., Yang, J.H., 2009. In-situ perovskite Sr–Nd isotopic constraints on the petrogenesis of the Ordovician Mengyin kimberlites in the North China craton. Chemical Geology 264, 24–42.

Zartman, R.E., Richardson, S.H., 2005. Evidence from kimberlitic zircon for a decreasing mantle Th/U since the Archean. Chemical Geology 220, 263–283.

Zhao, Z.F., Zheng, Y.F., 2007. Diffusion compensation for argon, hydrogen, lead, and strontium in minerals: empirical relationships to crystal chemistry. American Mineralogist 92, 289–308.

Zurevinski, S.E., Heaman, L.M., Creaser, R.A., Strand, P., 2008. The Churchill kimberlite field, Nunavut, Canada: petrology, mineral chemistry, and geochronology. Canadian Journal of Earth Sciences 45, 1039–1059.